THEORETICAL AND APPLIED MECHANICS
Volume 49 (2022) Issue 2, 183–221 DOI: https://doi.org/10.2298/TAM221115012K

AN EFFICIENT ALGORITHM FOR BIOMECHANICAL PROBLEMS BASED ON A FULLY IMPLICIT NESTED NEWTON SOLVER

Markus M. Knodel, Salvatore Di Stefano, Arne Nägel, and Alfio Grillo

Abstract. Numerical simulations of the dynamics of soft biological tissues are highly non-trivial because tissues generally exhibit complex biological response to external and internal actions, including large deformations and remodeling. Combining the advantages of globally implicit approach (GIA) solvers with the general applicability of the semi-implicit *General Plasticity Algorithm* (GPA), introduced by some of us some years ago, we present a new, efficient plasticity algorithm, which we call *Bio Mechanics Basis Plasticity Algorithm* (BMBPA). This is fully implicit, based on a nested Newton solver, and naturally suited for massively parallel computations. The Bilby–Kröner–Lee (BKL) multiplicative decomposition of the deformation gradient tensor is employed to introduce the unknowns of our model. We distinguish between global and local unknowns, associated with local and global equations, which are connected by means of a resolution function. The BMBPA asks for very few conditions to be applied and thus can be easily employed to solve several types of biological and biomechanical problems. We demonstrate the efficacy of BMBPA by performing two numerical experiments of a monophasic model of fiber-reinforced tissues. In one case, we consider the shear-compression test of a cubic specimen of tissue, while, in the other case, we focus on the unconfined compression test of a cylinder. The BMBPA is capable of solving the deformation and the remodeling of anisotropic biological tissues by employing a computation time of hours, while the GPA, applied to the same problems as the BMBPA, needs a substantially longer amount of time. All computations were performed in parallel and, within all tests, the performance of the BMBPA displayed substantially higher than the one of the GPA. The results of our simulations permit to study the overall mechanical behavior of the considered tissue and enable further investigations in the field of tissue biomechanics.

1991 *Mathematics Subject Classification:* 65M22; 65M50; 74-10; 74C15; 74S05.
Key words and phrases: nested Newton based algorithm, fiber-reinforced biological tissues, plastic-like distortions, computational biomechanics.

1. Introduction

The dynamics of biological tissues is dictated by the interactions exchanged with the surrounding environment and by complex physical processes ranging from the sub- and inter-cellular scales up to tissue scale [13, 14, 36, 37, 86]. As reported in [49], although a thorough treatment of this topic necessitates a multi-disciplinary approach, calling for the combination among processes of chemical, electrical and mechanical nature, in this paper we focus on Mechanics only.

We rely on mathematical models describing a class of mechanical processes according to which a tissue evolves in time by changing its shape and reorganizing its internal structure, in response to external stimuli and internal actions [13, 14, 36, 37, 49, 86]. In this respect, biological tissues are meant to undergo large deformations, which are generally accompanied by a structural evolution, the latter being a phenomenon known in the literature as remodeling [3, 4, 14, 23, 24, 37, 86, 89]. A remarkable feature of remodeling is that it is an anelastic process [49], which means that, also without external stimuli, a remodeled tissue can find itself in a stressed and/or distorted state [47, 49, 52, 83]. In fact, however, as is the case for plasticity, remodeling is responsible for redistributing the stress generated in a tissue in response to its structural transformations [49, 83].

In the present work, we study remodeling only, thereby neglecting phenomena such as growth or mass transfer, as the latter occur at time-scales sharply separated from those of remodeling. Such a situation is typical, for example, of biological systems such as cellular aggregates [21], in which the term remodeling accounts for processes like cell re-orientation and re-organization of the cell adhesion bonds [21, 41, 42, 47, 49], and fiber-reinforced soft tissues, like articular cartilage [15, 19, 46] or arteries [73], in which the structural changes of the extra-cellular matrix (ECM) feature an evolution of the fiber pattern. Other examples of remodeling phenomena are related to cell-matrix interactions mediated by focal adhesions, in terms of creation and rupture of bonds between cells and the adhesion plaque, as well as the adaptation of the protein structure of the latter [18, 20], and to bone tissue, explained in terms of irreversible formation of micro-cracks [38, 39, 74]. All these examples put in evidence that the type of remodeling considered in our work can be addressed by assuming the structural adaptation of a biological tissue to manifest as the onset and evolution of plastic-like distortions [19]. In other words, we assume the tissue to behave as an elasto-plastic medium [78], whose plastic-like distortions commence once a suitable measure of stress is greater than a threshold value [6, 42, 49, 78]. In light of this observation, it is possible to ascribe the study of remodeling within the setting of finite elasto-plasticity, and specialize to a biomechanical framework all the tools developed to study the elasto-plastic behavior of non-living matter [69, 72, 85]. Furthermore, such an analogy permits to employ the Bilby-Kröner-Lee (BKL) multiplicative decomposition of the deformation gradient tensor in order to decouple the contribution due to remodeling from that of elastic distortions [5, 7, 12, 22, 26, 48, 49, 51, 64, 68, 72, 77, 83, 84].

Given the complexity of the above introduced phenomena, reliable *in silico* predictions of biomechanical processes require advanced numerical techniques to

evaluate mathematical models in the context of realistic geometries and specialization to industrial and medical contexts [40, 76]. The numerical solution techniques which were developed for biomechanical questions took advantage of those already successfully applied to problems pertaining to the non-living world [1, 2, 9, 27, 53].

The so-called Return Mapping Algorithm (RMA) can be considered as the numerical "standard" method for addressing the numerical solution of mathematical models in the field of elasto-plasticity. In its original version, the RMA uses a projection method, usually based upon the hypothesis of isotropic elastoplastic material combined with an associative flow rule [85]. The RMA reduces the elasto-plastic model to a constrained optimization problem with a set of Karush-Kuhn-Tucker (KKT) conditions [85]. In a former study, Grillo et al. [49, 51] developed an algorithm, called General Plasticity Algorithm (GPA), for computing the elasto-plastic behavior of biological or non-living media and with the purpose of addressing more general modeling scenarios than those foreseen by RMA.

In this paper, we re-analyze the GPA and show that it is equivalent to an operator splitting method. This kind of methods often require many iterations between the two underlying nonlinear problems, as the error is shifted between the two sub-problems, and convergence problems may appear. This deficit turned out to create a major bottleneck for the evaluation of highly non-linear elasto-plastic models of anisotropic tissues.

To conclude, mathematical models of biomechanical deformations and elastic and plastic reorganizations of anisotropic tissue are very advanced. However, efficient solvers to evaluate these models are still needed.

For all theses reasons there is a need for the development of more efficient numerical solution techniques for biomechanical scenarios. This development should take advantage of the power of massively parallel supercomputers. As splitting sequential approaches like the GPA often bear restrictions, the Global Implicit Approach (GIA) is getting more important for solvers [8, 16, 17].

The crucial aspect of this work is to combine the advantages of the GPA with the advantages of monolithic fully globally implicit solvers and establish a new plasticity algorithm that applies with the same generality as the GPA, but also as efficiently as GIAs. In detail, we combine the same type of fully implicit nested Newton solver based on a resolution function as presented by Knodel et al. in [60] with the GPA. As our new algorithm presented in this study focuses upon Biomechanics questions, we call it Bio Mechanics Basic Plasticity Algorithm (BMBPA).

We apply the BMBPA to fiber-reinforced biological tissues undergoing remodeling. In particular, we would like to show how to simulate large deformations and plastic-like distortions in a robust manner, with the simulations performed within reasonable computing times.

We also consider the limit case of isotropy, in order to investigate the influence of the anisotropic material structure for deformation and plastic-like distortions based upon the GIA method introduced by us in this study into the field of elasto-plasticity. Hence, this study serves as a proof of concept of the new GIA based BMBPA algorithm, as the model of anisotropic tissue under deformation itself was

already published by us [51]. In particular, the BMBPA structure takes strong advantage of massively parallel computing facilities.

The manuscript is organized as follows. In Section 2, we present the general modeling background within which we study deformation and remodeling of biological tissues. In Section 3, we revisit the classical GPA, introduce the new fully implicit BMBPA, and compare the properties of both solvers. After describing the properties of the numerical experiments which we performed in Section 4, we present our simulation results in Section 5, and discuss these results in Section 6. The major conclusions are presented in Section 7. In Appendix A, we present the constitutive framework of the considered model.

2. Deformation and remodeling of biological tissues

We supply an idealized representation of a fiber-reinforced biological tissue, with respect to which the latter features two solid components: the extra-cellular matrix (ECM) and collagen fibers. Accordingly, we do not resolve the dynamics associated with the tissue's interstitial fluid, flowing throughout the tissue and saturating it. Such modeling choice, although neglects specific biological processes, still offers all the tools necessary to catch the most relevant aspects concerning the deformation and the remodeling of biological media.

In proposing this approach, we remark that the focus of our work is a novel algorithmic procedure aiming at efficiently solving dynamic problems of biological interest. In this sense, including the flow of the interstitial fluid in the model would lead, in general, to additional computational hurdles that, in fact, do not change the essence of the proposed solution algorithm. In addition, we mention that a similar approach, in which the interstitial fluid is neglected, has been recently employed to study multi-cellular aggregates as solid media, thereby neglecting the fluid phase [41]. In this case, the obtained results reproduce the experimental data in an excellent way [41].

In conclusion, a solid-phase model can represent a good compromise between a more specialized description of biological tissues and the computational issues that we aim at discussing, without being a strong restriction for the scopes of our work or for the generality of the designed algorithm.

2.1. Notation and kinematics. Let $\mathscr{B} \subset \mathscr{S}$ and $\mathscr{B}(t) \subset \mathscr{S}$ be the tissue's reference and current configuration at time $t \in \mathscr{I}$, with $\mathscr{S}$ and $\mathscr{I}$ being the three dimensional Euclidean space and a time interval. With a slight abuse of notation, we employ x and X to indicate both material points belonging to $\mathscr{S}$ and $\mathscr{B}$, respectively, and their coordinates. Moreover, we equip $\mathscr{S}$ and $\mathscr{B}$ with the metric tensors $\boldsymbol{g}(x,t)\colon T_x\mathscr{S} \to T_x^*\mathscr{S}$ and $\boldsymbol{G}(X,t)\colon T_X\mathscr{B} \to T_X^*\mathscr{B}$, with $\partial_t \boldsymbol{g}(x,t) = \boldsymbol{0}$ and $\partial_t \boldsymbol{G}(X,t) = \boldsymbol{0}$, where $T_X\mathscr{B}$ and $T_x\mathscr{S}$, and $T_X^*\mathscr{B}$ and $T_x^*\mathscr{S}$ are the tangent and the co-tangent spaces attached to $X \in \mathscr{B}$ and to $x \in \mathscr{S}$, respectively [70].

With a slight abuse of terminology, we introduce the tissue's motion $\chi(\cdot,t)\colon \mathscr{B} \to \mathscr{S}$, with $t \in \mathscr{I}$, as a time-dependent collection of embeddings [70], such that $\mathscr{B}(t) := \chi(\mathscr{B},t)$, and with its tangent map defining the deformation gradient tensor $D\chi(X,t) := \boldsymbol{F}(X,t)\colon T_X\mathscr{B} \to T_{\chi(X,t)}\mathscr{B}(t)$, with components $\boldsymbol{F}^a{}_A = [D\chi]^a{}_A = \chi^a{}_{;A}$. Moreover, the Jacobian of the latter, i.e., $J \equiv \det \boldsymbol{F} > 0$, is strictly positive.

2.2. The BKL decomposition. The tissue's remodeling, in the present paper, arises in terms of plastic-like distortions associated with the structural adaptation of the ECM's internal structure in response to external stimuli [41, 43, 49, 51]. In this respect, we describe the onset and evolution of such distortions by means of a *remodeling tensor* $\boldsymbol{F}_{\mathrm{p}}$, whose introduction stems from the BKL decomposition of the deformation gradient tensor $\boldsymbol{F}$, i.e.

$$\boldsymbol{F} = \boldsymbol{F}_{\mathrm{e}}\,\boldsymbol{F}_{\mathrm{p}}, \tag{2.1}$$

where $\boldsymbol{F}_{\mathrm{e}}$ is the *elastic distortions* tensor. Both $\boldsymbol{F}_{\mathrm{e}}$ and $\boldsymbol{F}_{\mathrm{p}}$ are non-singular, with their determinants $J_{\mathrm{e}} := \det \boldsymbol{F}_{\mathrm{e}}$ and $J_{\mathrm{p}} := \det \boldsymbol{F}_{\mathrm{p}}$ being strictly positive and such that $J = J_{\mathrm{e}} J_{\mathrm{p}}$. For a comprehensive treatment of the BKL decomposition, the reader is referred to [5, 7, 12, 22, 26, 48, 49, 51, 64, 68, 72, 77, 83, 84], while, in the following, we focus only on some specific aspects of this theory, with the scope of presenting the main features of the remodeling framework we adhere to.

The employment of the BKL decomposition relies on the fact that the tensor $\boldsymbol{F}_{\mathrm{p}}$ maps tangent vectors of the reference configuration (body elements) into body elements finding themselves in their natural state, i.e. $\boldsymbol{F}_{\mathrm{p}}(X,t)\colon T_X\mathscr{B} \to \mathscr{N}_X(t)$, where $\mathscr{N}_X(t)$ is a vector space collecting all the relaxed body elements attached to $X \in \mathscr{B}$ at time $t \in \mathscr{I}$. On the other hand, $\boldsymbol{F}_{\mathrm{e}}$ describes the elastic distortions necessary for $\mathscr{N}_X(t)$ to be mapped into $T_{\chi(X,t)}\mathscr{B}(t)$, i.e. $\boldsymbol{F}_{\mathrm{e}}(X,t)\colon \mathscr{N}_X(t) \to T_{\chi(X,t)}\mathscr{B}(t)$ (see [19, 22] and references therein).

Finally, by taking inspiration from [19, 25, 71], we introduce the *implant* tensor $\boldsymbol{K} = \boldsymbol{F}_{\mathrm{p}}^{-1}$ as the inverse of the remodeling tensor $\boldsymbol{F}_{\mathrm{p}}$, so that the decomposition in Equation (2.1) is re-written as

$$\boldsymbol{F}_{\mathrm{e}} = \boldsymbol{F}\,\boldsymbol{K}\,.$$

and with the determinant $J_{\boldsymbol{K}} := \det \boldsymbol{K} = 1/J_{\mathrm{p}}$.

2.3. Principle of Virtual Powers. In the quasi-static case, i.e., by neglecting inertia, and by assuming null long-range forces and tractions, acting on $\mathscr{B}$ and on the Neumann boundary of $\mathscr{B}$, $\partial_N\mathscr{B}$, respectively, the Principle of Virtual Powers can be stated as [51]

$$\int_{\mathscr{B}} \boldsymbol{P} : \mathfrak{g}\,\mathrm{Grad}\,\tilde{\boldsymbol{v}} = 0. \tag{2.2}$$

In Equation (2.2), $\boldsymbol{P}(X,t)\colon T_X\mathscr{B} \to T_{\chi(X,t)}\mathscr{S}$ is the first Piola Kirchhoff stress tensor, $\mathfrak{g}(X,t) = \boldsymbol{g}(\chi(X,t),t)$ is the spatial metric tensor evaluated along the motion χ and $\tilde{\boldsymbol{v}}\colon \mathscr{B} \to T\mathscr{S}$ is a field of virtual velocities such that $\tilde{\boldsymbol{v}}_{|\partial_D\mathscr{B}} = \boldsymbol{0}$. Here, $\partial_D\mathscr{B}$ is the Dirichlet boundary of $\mathscr{B}$, i.e., the portion of the boundary of $\mathscr{B}$ over which Dirichlet boundary conditions of the type $\chi = \chi_{\mathrm{D}}$ are enforced and $T\mathscr{S}$ is the bundle $T\mathscr{S} = \sqcup_{x\in\mathscr{S}} T_x\mathscr{S}$. Finally, we recall that $\partial\mathscr{B} = \partial_D\mathscr{B} \cup \partial_N\mathscr{B}$ and $\overline{\partial_D\mathscr{B}} \cap \partial_N\mathscr{B} = \partial_D\mathscr{B} \cap \overline{\partial_N\mathscr{B}} = \emptyset$, where an superimposed bar denotes the topological closure of a set.

In the following, we regard the biological tissue under study as hyperelastic and, thus, we postulate the existence of a strain energy density function, hereafter denoted by ψ_{R}. In particular, we consider the case in which the information on the

material behavior described by ψ_{R} is given in terms of $\boldsymbol{F}$ and $\boldsymbol{K}$. Hence, we write $\psi_{\mathrm{R}} = \hat{\psi}_{\mathrm{R}} \circ (\boldsymbol{F}, \boldsymbol{K})$ and express the first Piola–Kirchhoff stress tensor as

$$\boldsymbol{P} = \hat{\boldsymbol{P}} \circ (\boldsymbol{F}, \boldsymbol{K}) = \frac{\partial \hat{\psi}_{\mathrm{R}}}{\partial \boldsymbol{F}} \circ (\boldsymbol{F}, \boldsymbol{K}).$$

We remark that the explicit dependence of ψ_{R} on material points X is understood but omitted, to maintain the notation as lighter as possible. A discussion related to this aspect is reported in Appendix A.

2.4. Remodeling law. With reference to [19], we start considering, for exemplification purposes, the following remodeling law

$$\operatorname{sym}(\boldsymbol{\Lambda}\, \boldsymbol{C}^{-1}) = -\zeta[\boldsymbol{S} - \tfrac{1}{3} \operatorname{tr}(\boldsymbol{C}\, \boldsymbol{S})\, \boldsymbol{C}^{-1}], \tag{2.3}$$

where $\boldsymbol{\Lambda} = \dot{\boldsymbol{K}}\, \boldsymbol{K}^{-1}$ is the tensor of rate of remodeling [19], $\boldsymbol{S}$ is the second Piola–Kirchhoff stress tensor, related to the first Piola–Kirchhoff stress tensor $\boldsymbol{P}$ by $\boldsymbol{P} = \boldsymbol{F}\, \boldsymbol{S}$, $\boldsymbol{C}(X,t) = \boldsymbol{F}^{\mathrm{T}}(\chi(X,t),t)\mathfrak{g}(X,t)\, \boldsymbol{F}(X,t)$ is the right Cauchy-Green deformation tensor and ζ is a non-negative term determining the activation of the evolution of $\boldsymbol{K}$, which is assumed to coincide with the symmetric part of its polar decomposition, and is hereafter denoted by $\boldsymbol{K}$ itself. In particular, we set [19]

$$\zeta = \frac{1}{J_{\boldsymbol{K}}} \lambda \left[\frac{\| \operatorname{dev} \boldsymbol{\sigma} \| - \sqrt{2/3}\sigma_{\mathrm{y}}}{\| \operatorname{dev} \boldsymbol{\sigma} \|} \right]_{+}, \tag{2.4}$$

where λ and σ_{y} are positive material parameters accounting for the time scale at which remodeling occurs and the yield stress of the tissue, respectively [41, 42]. In addition, the operator $[\,\cdot\,]_{+}$ returns the positive part of its argument, so that $\zeta = 0$ if $\| \operatorname{dev} \boldsymbol{\sigma} \| \leqslant \sqrt{2/3}\sigma_{\mathrm{y}}$ and $\zeta > 0$ if $\| \operatorname{dev} \boldsymbol{\sigma} \| > \sqrt{2/3}\sigma_{\mathrm{y}}$. Finally, $\| \operatorname{dev} \boldsymbol{\sigma} \|$ is the norm of the deviatoric part of Cauchy stress tensor, $\boldsymbol{P} = J\boldsymbol{\sigma}\boldsymbol{F}^{-\mathrm{T}}$, where, with a slight abuse of notation, $\boldsymbol{\sigma}$ is understood as a function of material points. In particular, we have

$$\| \operatorname{dev} \boldsymbol{\sigma} \| = \sqrt{\operatorname{tr}[(\boldsymbol{g} \operatorname{dev} \boldsymbol{\sigma})^2]},$$
$$\operatorname{dev} \boldsymbol{\sigma} = \boldsymbol{\sigma} - \tfrac{1}{3} \operatorname{tr}(\boldsymbol{g}\boldsymbol{\sigma})\boldsymbol{g}^{-1}.$$

Also Cauchy stress $\boldsymbol{\sigma}$ can be constitutively expressed as a function of $\boldsymbol{F}$ and $\boldsymbol{K}$, i.e., $\boldsymbol{\sigma} = \hat{\boldsymbol{\sigma}} \circ (\boldsymbol{F}, \boldsymbol{K})$. Accordingly, by virtue of Equation (2.4), we employ the notation $\zeta = \hat{\zeta} \circ (\boldsymbol{F}, \boldsymbol{K})$. We remark that Equation (2.3) can be recast in a much more general form, which is meant to cover a wider range of remodeling phenomena. Hence, we write

$$\mathcal{T}[\boldsymbol{F}, \boldsymbol{K}] + [\hat{\zeta} \circ (\boldsymbol{F}, \boldsymbol{K})][\hat{\boldsymbol{M}} \circ (\boldsymbol{F}, \boldsymbol{K})] = \boldsymbol{0}, \tag{2.5}$$

where $\hat{\zeta} \circ (\boldsymbol{F}, \boldsymbol{K})$ is a non-negative activation factor, $\hat{\boldsymbol{M}} \circ (\boldsymbol{F}, \boldsymbol{K})$ is a measure of stress driving remodeling, such as Mandel stress, $\boldsymbol{\Sigma} = \boldsymbol{C}\boldsymbol{S}$, or its deviatoric part, and the operator $\mathcal{T}[\boldsymbol{F}, \boldsymbol{K}]$ is a short-hand notation to denote

$$\mathcal{T}[\boldsymbol{F}, \boldsymbol{K}] = \hat{\mathcal{T}} \circ (\boldsymbol{F}, \boldsymbol{K}, \dot{\boldsymbol{K}}),$$
$$\mathcal{T}_{(X,t)}[\boldsymbol{F}, \boldsymbol{K}] = \hat{\mathcal{T}}(\boldsymbol{F}(X,t), \boldsymbol{K}(X,t), \dot{\boldsymbol{K}}(X,t)).$$

It is important to remark that the proposed algorithm, i.e. the BMBPA, is general enough to be independent of the specific form of Equation (2.3). Moreover, Equation (2.5) and the BMBPA comply with a rather general constitutive framework and with the case of non-vanishing external power. Finally, it is worth to mention that the BMBPA is independent of the assumption of symmetric remodeling variables.

2.5. General formulation of the model. Equations (2.2) and (2.3) give rise to the system of fully coupled, non-linear, equations

$$0 = \mathcal{P}[\chi, \boldsymbol{K}] = \mathfrak{P}[\boldsymbol{F}, \boldsymbol{K}], \tag{2.6a}$$

$$\boldsymbol{0} = \mathcal{G}[\chi, \boldsymbol{K}] = \mathfrak{G}[\boldsymbol{F}, \boldsymbol{K}], \tag{2.6b}$$

where the functionals $\mathfrak{P}$ and $\mathfrak{G}$ are defined by

$$\mathfrak{P}[\boldsymbol{F}, \boldsymbol{K}] := \int_{\mathscr{B}} \hat{\boldsymbol{P}} \circ (\boldsymbol{F}, \boldsymbol{K}) : \mathfrak{g}\mathrm{Grad}\tilde{\boldsymbol{v}}, \tag{2.7a}$$

$$\mathfrak{G}[\boldsymbol{F}, \boldsymbol{K}] := \mathcal{T}[\boldsymbol{F}, \boldsymbol{K}] + [\hat{\zeta} \circ (\boldsymbol{F}, \boldsymbol{K})][\hat{\boldsymbol{M}} \circ (\boldsymbol{F}, \boldsymbol{K})], \tag{2.7b}$$

and, for the sake of a lighter notation, we omit the functional dependence of $\mathfrak{P}$ on the test function $\tilde{\boldsymbol{v}}$. We recall that, in light of the flow rule in Equation (2.3), in this work we set

$$\mathfrak{G}[\boldsymbol{F}, \boldsymbol{K}] = \mathrm{sym}(\boldsymbol{\Lambda}\, \boldsymbol{C}^{-1}) + \hat{\zeta} \circ (\boldsymbol{F}, \boldsymbol{K})[\hat{\boldsymbol{S}} \circ (\boldsymbol{F}, \boldsymbol{K}) - \tfrac{1}{3}\, \mathrm{tr}(\boldsymbol{C}\, \hat{\boldsymbol{S}} \circ (\boldsymbol{F}, \boldsymbol{K}))\boldsymbol{C}^{-1}]. \tag{2.8}$$

We notice that Equations (2.7a) and (2.7b) involve, in general, twelve scalar unknowns, i.e., the three components of χ and the nine components of $\boldsymbol{K}$. However, in the present work, the unknowns reduce to eight, with only five independent components of $\boldsymbol{K}$, since $\boldsymbol{K}$ is isochoric, i.e., $J_{\boldsymbol{K}} = 1$, and symmetric.

Finally, we remark that, in the present framework, the Principle of Virtual Powers, expressing the weak form of the balance of linear momentum, does not involve time derivatives of χ. On the other hand, the flow rule in Equation (2.3) features a term containing the time derivative of $\boldsymbol{K}$ and another summand depending on $\boldsymbol{F}$ and $\boldsymbol{K}$ only, representing the activation and the stress-driven evolution of remodeling.

For a list containing the main kinematic and stress-like quantities and their respective symbols used in this study, we refer to Table 2 (see the last part of Appendix A).

2.6. Global and local system and variables. In the proposed formulation of the Principle of Virtual Powers, no generalized velocity associated with $\boldsymbol{K}$ appears, because $\boldsymbol{K}$ is regarded as an internal variable [51] whose corresponding equation, i.e., the flow rule in Equation (2.7b), is not put in weak form. Indeed, the problem consists of the integral form of a second-order partial differential equation (PDE) in the space variables, i.e., Equation (2.7a), and of Equation (2.7b), which is a tensorial ordinary differential equation (ODE) of the first order in time and applies point-wise. This leads to a different interpretation of the equations and reflects the way in which they are solved numerically.

If we take into account that PDEs contain spatial couplings, whereas ODEs do not contain such couplings, it is tempting to say that Equation (2.7a) leads to a *global* system, whereas Equation (2.7b) might be said to yield a *local* system, as already performed in [60]. Conventionally, we call "global" variables those variables solved by the global equations, while we define "local" variables those variables that are solved by the local equations. In this respect, the motion χ is global, while $\boldsymbol{K}$ is local. For future use, we refer to $\boldsymbol{F}$ as a global auxiliary variable, since it is obtained through χ, which is global. To summarize this, we visualize the correspondence between the types of unknowns and the associated equations as follows

Type of equation	Equations	Reference	Variables
Global	$\mathfrak{P}[\boldsymbol{F}, \boldsymbol{K}] = 0$	Equation(2.6a)	$\boldsymbol{F} = D\chi \equiv \boldsymbol{F}[\chi]$
Local	$\mathfrak{G}[\boldsymbol{F}, \boldsymbol{K}] = \boldsymbol{0}$	Equation(2.6b)	$\boldsymbol{K}$

where the notation $\boldsymbol{F}[\chi]$ indicates that $\boldsymbol{F}$ is computed as an operator acting on χ.

3. Computational framework and solution algorithm: the BMBPA

We propose a computational algorithm which we call *Bio Mechanics Basis Plasticity Algorithm* (BMBPA), and, in the present work, we employ it to address a class of problems in the field of Biomechanics. In particular, we specialize our study to fiber-reinforced biological tissues undergoing finite deformations and remodeling, the latter describing the anelastic evolution of the considered tissue's internal structure. We remark that the word "plasticity" contained in the name of the proposed algorithm descends from the fact that we study biological remodeling by having recourse to the theory of elastoplasticity, as explained in the previous sections. Moreover, this evidence highlights the possibility of employing the BMBPA within non-biological contexts, as is the case, for instance, of plastic distortions occurring in non-living matter of industrial interest.

3.1. Overview. In designing our computational approach, we appropriately consider the non-linearities related to the tissue's kinematics and to the employed constitutive laws. Moreover, we also account for fibers, thereby implying the necessity of considering anisotropy, which represents a step forward with respect to other computational strategies [49, 51].

Before going further, we highlight that the BMBPA places itself as a generalization of some numerical schemes available in the literature and it features several developments with respect to them. In particular, it aims at proposing new solution approaches, which permit to include innovative discretization rules and linearization algorithms. As a reference case, we mainly look upon the *Generalised Plasticity Algorithm* (GPA) developed in [49, 51], as a term of comparison to show the peculiarities and the novelties of BMBPA.

We will briefly discuss a review of the GPA and we highlight the main reasons for which a generalization to the BMBPA is required. Afterwards, we present the BMBPA, a new and fully implicit, nested Newton based algorithm. In fact, the BMBPA takes large inspiration and contains ideas from the GPA, but enriches and improves its computational characteristics by calling for principles of fully implicit algorithms and nested Newton procedures.

3.2. Partial and total Gâteaux derivative of operators. As discussed above, Equations (2.7) bring about a system of highly non-linear equations, whose numerical solution calls for Newton-like procedures to linearize the Principle of Virtual Powers and the flow rule. For future use, we here introduce the notation relative to the functional derivative of operators of the same type as those appearing in Equations (2.6) and (2.7). We remark that, although under a different role, the notion of functional derivative will be used both in the case of GPA and in the case of BMBPA.

Let us introduce an operator $\mathfrak{A}[\cdot,\cdot]$, and let us consider the evaluation of $\mathfrak{A}$ in correspondence of two tensors, $\boldsymbol{X}$ and $\boldsymbol{Y}$, so that we write $\mathfrak{A}[\boldsymbol{X},\boldsymbol{Y}]$. By adopting a standard notation, we define the partial Gâteaux derivatives with respect to $\boldsymbol{X}$ and $\boldsymbol{Y}$, along the increments $\boldsymbol{\Delta_X}$ and $\boldsymbol{\Delta_Y}$, as

$$\partial_{\boldsymbol{X}}\mathfrak{A}[\boldsymbol{X},\boldsymbol{Y};\boldsymbol{\Delta_X}] := \left[\frac{\mathrm{d}}{\mathrm{d}\varepsilon}\mathfrak{A}[\boldsymbol{X}+\varepsilon\boldsymbol{\Delta_X},\boldsymbol{Y}]\right]\Big|_{\varepsilon=0},$$
$$\partial_{\boldsymbol{Y}}\mathfrak{A}[\boldsymbol{X},\boldsymbol{Y};\boldsymbol{\Delta_Y}] := \left[\frac{\mathrm{d}}{\mathrm{d}\varepsilon}\mathfrak{A}[\boldsymbol{X},\boldsymbol{Y}+\varepsilon\boldsymbol{\Delta_Y}]\right]\Big|_{\varepsilon=0},$$

with ε being a positive smallness parameter. In some cases, the notation with bra-ket may be employed, so that one can write [10]

$$\partial_{\boldsymbol{X}}\mathfrak{A}[\boldsymbol{X},\boldsymbol{Y};\boldsymbol{\Delta_X}] \equiv \langle\partial_{\boldsymbol{X}}\mathfrak{A}[\boldsymbol{X},\boldsymbol{Y}]|\boldsymbol{\Delta_X}\rangle,$$
$$\partial_{\boldsymbol{Y}}\mathfrak{A}[\boldsymbol{X},\boldsymbol{Y};\boldsymbol{\Delta_Y}] \equiv \langle\partial_{\boldsymbol{Y}}\mathfrak{A}[\boldsymbol{X},\boldsymbol{Y}]|\boldsymbol{\Delta_Y}\rangle,$$

thereby highlighting that $\partial_{\boldsymbol{X}}\mathfrak{A}[\boldsymbol{X},\boldsymbol{Y}]$ and $\partial_{\boldsymbol{Y}}\mathfrak{A}[\boldsymbol{X},\boldsymbol{Y}]$ are linear functionals of $\Delta_{\boldsymbol{X}}$ and $\Delta_{\boldsymbol{Y}}$, respectively. Moreover, if we suppose the tensor $\boldsymbol{Y}$ to be a function of the tensor $\boldsymbol{X}$, we write $\boldsymbol{Y}=\hat{\boldsymbol{Y}}(\boldsymbol{X})$ and $\hat{\mathfrak{A}}[\boldsymbol{X}]=\mathfrak{A}[\boldsymbol{X},\hat{\boldsymbol{Y}}(\boldsymbol{X})]$. Hence, the total Gâteaux derivative of $\hat{\mathfrak{A}}$ along the increment $\boldsymbol{\Delta_X}$ is defined as

$$\begin{aligned}(3.1)\quad \mathrm{D}_{\boldsymbol{X}}\hat{\mathfrak{A}}[\boldsymbol{X};\boldsymbol{\Delta_X}] :&= \left[\frac{\mathrm{d}}{\mathrm{d}\varepsilon}\hat{\mathfrak{A}}[\boldsymbol{X}+\varepsilon\boldsymbol{\Delta_X}]\right]\Big|_{\varepsilon=0}\\ &= \left[\frac{\mathrm{d}}{\mathrm{d}\varepsilon}\mathfrak{A}[\boldsymbol{X}+\varepsilon\boldsymbol{\Delta_X},\hat{\boldsymbol{Y}}(\boldsymbol{X}+\varepsilon\boldsymbol{\Delta_X})]\right]\Big|_{\varepsilon=0}\\ &= \partial_{\boldsymbol{X}}\mathfrak{A}[\boldsymbol{X},\hat{\boldsymbol{Y}}(\boldsymbol{X});\boldsymbol{\Delta_X}] + \partial_{\boldsymbol{Y}}\mathfrak{A}[\boldsymbol{X},\hat{\boldsymbol{Y}}(\boldsymbol{X});\underbrace{\mathrm{D}_{\boldsymbol{X}}\hat{\boldsymbol{Y}}[\boldsymbol{X};\boldsymbol{\Delta_X}]}_{\equiv\boldsymbol{\Delta_Y}}],\end{aligned}$$

for which we can use the equivalent bra-ket notation

$$\begin{aligned}(3.2)\quad \mathrm{D}_{\boldsymbol{X}}\hat{\mathfrak{A}}[\boldsymbol{X};\boldsymbol{\Delta_X}] &\equiv \langle\mathrm{D}_{\boldsymbol{X}}\hat{\mathfrak{A}}[\boldsymbol{X}]|\boldsymbol{\Delta_X}\rangle\\ &= \langle\partial_{\boldsymbol{X}}\mathfrak{A}[\boldsymbol{X},\hat{\boldsymbol{Y}}(\boldsymbol{X})]|\boldsymbol{\Delta_X}\rangle + \langle\partial_{\boldsymbol{Y}}\mathfrak{A}[\boldsymbol{X},\hat{\boldsymbol{Y}}(\boldsymbol{X})].\mathrm{D}_{\boldsymbol{X}}\hat{\boldsymbol{Y}}(\boldsymbol{X})|\boldsymbol{\Delta_X}\rangle.\end{aligned}$$

We remark that in Equation (3.2) the dot "." indicates a composition of linear maps whose result is applied to $\boldsymbol{\Delta_X}$. When $\mathfrak{A}$ is a second-order tensor, as is the case for the flow rule (see Section 3.3.1), the dot means a double-contraction between fourth-order tensors, and its result is applied to $\boldsymbol{\Delta_X}$. On the other hand, when $\mathfrak{A}$ is defined through an integral, as is the case for the internal virtual power, the expression $\langle\partial_{\boldsymbol{Y}}\mathfrak{A}[\boldsymbol{X},\hat{\boldsymbol{Y}}(\boldsymbol{X})].\mathrm{D}_{\boldsymbol{X}}\hat{\boldsymbol{Y}}(\boldsymbol{X})|\boldsymbol{\Delta_X}\rangle$ is intended in the sense explained in Equations (3.6a)–(3.6c) through (3.7). Note that due to the fact that $\hat{\boldsymbol{Y}}(\boldsymbol{X})$ is only a function of $\boldsymbol{X}$, the partial and the total derivative match, i.e. $\mathrm{D}_{\boldsymbol{X}}\hat{\boldsymbol{Y}}(\boldsymbol{X}) = \partial_{\boldsymbol{X}}\hat{\boldsymbol{Y}}(\boldsymbol{X})$.

3.3. Review of the GPA. The formulation of the GPA, as well as its employment to numerically solve dynamical problems of biological interest, has been presented in [51]. In particular, in our paper, we consider modeling equations analogous to those reported in [51]. In this respect, also in [51], the model equations are put in a form similar to that of Equations (2.6), with the consequent arising of a global and of a local problem, according to the definitions given in Section 2.6 and taking inspiration from [60]. Although in [51] the terminologies *"global problem"* and *"local problem"* are not employed to denote the weak form of the balance of linear momentum and the flow rule, respectively, in the present paper we will refer to GPA by adapting our wordings to it.

The main characteristic of the GPA is the application of a two-step linearization procedure, based on Newton method. More specifically, Equations (2.6) are not linearized together, but each of Equations (2.6a) and (2.6b) is linearized following an independent rationale. Such a distinction relies on the diverse physical conception leading to the formulation of Equations (2.6a) and (2.6b), as discussed in Section 2. We anticipate that, within the formulation of the BMBPA, the difference with respect to which Equation (2.6a) and Equation (2.6b) are conceived is one of the key points of the algorithm.

In order to give a schematic description of the GPA, we remark that the starting point of this algorithm consists of numerically solving the local system. This produces a tentative solution value for $\boldsymbol{K}$ that, according to the iterative nature of Newton method, should be tested by means of a convergence criterion (see Algorithm 1). As a second step, the solution of the global problem is computed, while no direct convergence criterion is imposed. By invoking a further convergence criterion, also the update of the local variable is reached.

As a detailed explanation of the GPA is furnished in [51], hereafter we discuss its most important aspects, in light of providing a comparison with the BMBPA.

In the following, we call *global Newton step* and *local Newton step* the linearization procedure leading to the solution of the global and of the local problem, respectively. In addition, by considering to know the value of $\boldsymbol{F}$ at the $(k-1)$th interaction of the global Newton step, $\boldsymbol{F}_{k-1}$, with $k \geqslant 1$, and the value of $\boldsymbol{K}$ at the $(\ell-1)$th interaction of the local Newton step, $\boldsymbol{K}_{\ell-1}$, with $\ell \geqslant 1$, we set

$$\begin{aligned} \boldsymbol{F}_k &:= \boldsymbol{F}_{k-1} + \Delta^k_{\boldsymbol{F}}, \\ \boldsymbol{K}_\ell &:= \boldsymbol{K}_{\ell-1} + \Delta^\ell_{\boldsymbol{K}}, \end{aligned}$$

where $\Delta^k_{\boldsymbol{F}}$ and $\Delta^\ell_{\boldsymbol{K}}$ are the increments relative to $\boldsymbol{F}$ and $\boldsymbol{K}$ that must be computed to update the solutions at the kth interaction of the global Newton step and at the ℓth interaction of the local Newton step.

3.3.1. *Solution of the local system.* Following [49, 51], we compute $\Delta^\ell_{\boldsymbol{K}}$ at the ℓth iteration of the local Newton step as a solution of the problem

$$\mathbb{J}^{\mathrm{loc}}_{\mathrm{GPA}}[\boldsymbol{F}_{k-1}, \boldsymbol{K}_{\ell-1}] : \Delta^\ell_{\boldsymbol{K}} = -\boldsymbol{R}^{\mathrm{loc}}_{\mathrm{GPA}}[\boldsymbol{F}_{k-1}, \boldsymbol{K}_{\ell-1}], \tag{3.3}$$

where $\mathbb{J}^{\mathrm{loc}}_{\mathrm{GPA}}$ and $\boldsymbol{R}^{\mathrm{loc}}_{\mathrm{GPA}}$ are the local Jacobian and the local residuum, defined as

$$\mathbb{J}^{\mathrm{loc}}_{\mathrm{GPA}}[\boldsymbol{F}, \boldsymbol{K}] := \partial_{\boldsymbol{K}} \mathfrak{G}[\boldsymbol{F}, \boldsymbol{K}], \tag{3.4a}$$

$$\boldsymbol{R}^{\mathrm{loc}}_{\mathrm{GPA}}[\boldsymbol{F},\boldsymbol{K}] := \mathfrak{G}[\boldsymbol{F},\boldsymbol{K}]. \tag{3.4b}$$

In Equations (3.4a), $\mathbb{J}^{\mathrm{loc}}_{\mathrm{GPA}}[\boldsymbol{F},\boldsymbol{K}]$ is a fourth-order tensor, computed as the partial Gâteaux derivative of $\mathfrak{G}$ with respect to $\boldsymbol{K}$, while $\boldsymbol{R}^{\mathrm{loc}}_{\mathrm{GPA}}[\boldsymbol{F},\boldsymbol{K}]$ is a second-order tensor, giving an estimate of the solutions computed as outputs of the global and local steps of the adopted two-step Newton procedure.

3.3.2. *Solution of the global system.* The lth iteration of the global Newton step leads to the determination of $\Delta^k_{\boldsymbol{F}}$ by considering the numerical solution of the problem:

$$J^{\mathrm{glob}}_{\mathrm{GPA}}[\boldsymbol{F}_{k-1},\boldsymbol{K}_{\ell-1};\Delta_{\boldsymbol{F}^k}] = -R^{\mathrm{glob}}_{\mathrm{GPA}}[\boldsymbol{F}_{k-1},\boldsymbol{K}_{\ell-1};\Delta^{\ell}_{\boldsymbol{K}}], \tag{3.5}$$

where the global Jacobian functional $J^{\mathrm{glob}}_{\mathrm{GPA}}$ and the global residuum functional $\boldsymbol{R}^{\mathrm{glob}}_{\mathrm{GPA}}$ are defined by

$$J^{\mathrm{glob}}_{\mathrm{GPA}}[\boldsymbol{F},\boldsymbol{K};\Delta^k_{\boldsymbol{F}}] := \int_{\mathscr{B}} \mathfrak{g}\,\mathrm{Grad}\,\tilde{\boldsymbol{v}} : \mathbb{J}^{\mathrm{glob}}_{\mathrm{GPA}}[\boldsymbol{F},\boldsymbol{K}] : \Delta^k_{\boldsymbol{F}} \tag{3.6a}$$

$$\mathbb{J}^{\mathrm{glob}}_{\mathrm{GPA}}[\boldsymbol{F},\boldsymbol{K}] := \partial_{\boldsymbol{F}}\hat{\boldsymbol{P}} \circ (\boldsymbol{F},\boldsymbol{K}) - \partial_{\boldsymbol{F}}[\partial_{\boldsymbol{K}}\hat{\boldsymbol{P}} \circ (\boldsymbol{F},\boldsymbol{K}) : (\partial_{\boldsymbol{K}}\mathfrak{G}[\boldsymbol{F},\boldsymbol{K}])^{-1} : \mathfrak{G}(\boldsymbol{F},\boldsymbol{K})], \tag{3.6b}$$

$$R^{\mathrm{glob}}_{\mathrm{GPA}}[\boldsymbol{F},\boldsymbol{K};\Delta^{\ell}_{\boldsymbol{K}}] := \mathfrak{P}[\boldsymbol{F},\boldsymbol{K}] + \langle \partial_{\boldsymbol{K}}\mathfrak{P}[\boldsymbol{F},\boldsymbol{K}] | \Delta^{\ell}_{\boldsymbol{K}} \rangle, \tag{3.6c}$$

where $\mathbb{J}^{\mathrm{glob}}_{\mathrm{GPA}}[\boldsymbol{F},\boldsymbol{K}]$ is the fourth-order tensor that defines the global Jacobian functional and represents also a "rescaled" first elasticity tensor [51]. Since it holds that $\Delta^k_{\boldsymbol{F}} := \mathrm{Grad}\,\boldsymbol{h}^k$, with $\boldsymbol{h}^k$ being the increment associated with the motion χ^{k-1}, Equation (3.6a) is indeed the bilinear form [51]

$$a(\tilde{\boldsymbol{v}},\boldsymbol{h}^k) = \int_{\mathscr{B}} \mathfrak{g}\,\mathrm{Grad}\,\tilde{\boldsymbol{v}} : \mathbb{J}^{\mathrm{glob}}_{\mathrm{GPA}}[\boldsymbol{F},\boldsymbol{K}] : \mathrm{Grad}\,\boldsymbol{h}^k$$

adopted to express the abstract form of the considered finite element method [58]. However, for the sake of a compact notation, we write

$$J^{\mathrm{glob}}_{\mathrm{GPA}}[\boldsymbol{F},\boldsymbol{K};\Delta^k_{\boldsymbol{F}}] \equiv a(\tilde{\boldsymbol{v}},\boldsymbol{h}^k) \equiv \left\langle J^{\mathrm{glob}}_{\mathrm{GPA}}[\boldsymbol{F},\boldsymbol{K}] | \Delta^k_{\boldsymbol{F}} \right\rangle,$$

where, with abuse of notation, $J^{\mathrm{glob}}_{\mathrm{GPA}}[\boldsymbol{F},\boldsymbol{K}]$ is understood as

$$J^{\mathrm{glob}}_{\mathrm{GPA}}[\boldsymbol{F},\boldsymbol{K}] := \partial_{\boldsymbol{F}}\mathfrak{P}[\boldsymbol{F},\boldsymbol{K}] - \partial_{\boldsymbol{F}}\{\partial_{\boldsymbol{K}}\mathfrak{P}[\boldsymbol{F},\boldsymbol{K}].(\partial_{\boldsymbol{K}}\mathfrak{G}[\boldsymbol{F},\boldsymbol{K}])^{-1} : \mathfrak{G}(\boldsymbol{F},\boldsymbol{K})\}. \tag{3.7}$$

3.3.3. *Algorithm 1: GPA.* Algorithm 1 displays and summarizes the ordering of the Newton steps in case of the GPA. We remark that, within Algorithm 1, we use the subscript "n" to highlight that all the variables are computed at the instant of time t_n, once a discretization in time is introduced (see the following Section 4). In brief, at each time step, the starting point of the GPA is the tentative solution of the local system; by employing this tentative solution, the global update is computed and, by invoking specific convergence criteria also the local variable is updated (see [51] for all the details).

Algorithm 1 GPA algorithm for one single time step with the focus upon the two Newton procedures, assuming that the result of the former time step $\boldsymbol{F}_{n-1}$ and $\boldsymbol{K}_{n-1}$ is known (as initial value in case that $n = 1$ or computed for the case $n > 1$ with the given algorithm).

$k = \ell = 1$, $\boldsymbol{F}_{n,k-1} = \boldsymbol{F}_{n-1}$, $\boldsymbol{K}_{n,\ell-1} = \boldsymbol{K}_{n-1}$ ▷ start time step, assign initial values
$[\mathbb{J}^{\text{loc}}_{\text{GPA}}[\boldsymbol{F}_{n,k-1}, \boldsymbol{K}_{n,\ell-1}]] : \Delta^{\ell}_{\boldsymbol{K}} = -\boldsymbol{R}^{\text{loc}}_{\text{GPA}}[\boldsymbol{F}_{n,k-1}, \boldsymbol{K}_{n,\ell-1}]$
▷ solve local system (3.3), tentative update $\Delta_{\boldsymbol{K}}$-but *no* local update
if $R_{\text{glob}} = \|R^{\text{glob}}_{\text{GPA}}[\boldsymbol{F}_{n,k-1}, \boldsymbol{K}_{n,\ell-1}; \Delta^{\ell}_{\boldsymbol{K}}]\| > \epsilon_G$ **then** ▷ global residuum (3.6c) has not converged
  $J^{\text{glob}}_{\text{GPA}}[\boldsymbol{F}_{n,k-1}, \boldsymbol{K}_{n,\ell-1}; \Delta^{k}_{\boldsymbol{F}}] = -R^{\text{glob}}_{\text{GPA}}[\boldsymbol{F}_{n,k-1}, \boldsymbol{K}_{n,\ell-1}; \Delta^{\ell}_{\boldsymbol{K}}]$ ▷ solve global system (3.5)
  $\boldsymbol{F}_{n,k} = \boldsymbol{F}_{n,k-1} + \Delta^{k}_{\boldsymbol{F}}$ ▷ global Newton step-accept
  $k = k + 1$, **go to** 2 ▷ start next *global* Newton round
else ▷ global residuum converged, $R_{\text{glob}} < \epsilon_G$
  $\boldsymbol{K}_{n,\ell} = \boldsymbol{K}_{n,\ell-1} + \Delta^{\ell}_{\boldsymbol{K}}$ ▷ local Newton step-accept
  if $R_{\text{loc}} = \|\boldsymbol{R}^{\text{loc}}_{\text{GPA}}[\boldsymbol{F}_{n,k-1}, \boldsymbol{K}_{n,\ell}]\| > \epsilon_L$ **then** ▷ local residuum (3.4b) has not converged
    $\ell = \ell + 1$, **go to** 2 ▷ start next *global* Newton round
  else ▷ local residdum converged, $R_{\text{loc}} < \epsilon_L$
    $\boldsymbol{F}_n = \boldsymbol{F}_{n,k}$, $\boldsymbol{K}_n = \boldsymbol{K}_{n,\ell}$, $n = n + 1$, **go to** 1 ▷ time step finished
  end if ▷ no check of R_{glob} with updated $\boldsymbol{K}$
end if

3.3.4. *Features and limitations of the GPA.* The following properties can be deduced:

- Formally, GPA is an operator splitting method. It consists of two parallel (non-nested) Newton procedures, treating local and global variables equally.
- While each ℓth local and kth global Newton step starts with a new computation of $\Delta^{\ell}_{\boldsymbol{K}}$, this value does *not* automatically lead to an update $\boldsymbol{K}_{n,\ell} = \boldsymbol{K}_{n,\ell-1} + \Delta^{\ell}_{\boldsymbol{K}}$ (as long as the global residuum does not converge).
- Note that, after each global Newton step of the GPA, the convergence w.r.t global residuum is *not* checked immediately. Instead, a tentative local correction is computed and convergence is tested based on a linearized version of the global residual.
- Note that the global residuum is never checked with entirely updated remodeling variables, but only with the first order of the Taylor expansion of the Principle of Virtual Powers w.r.t. the remodeling variable. Assuming one global and one local Newton step performed (i.e. assuming that one global Newton step was sufficient to induce one local Newton step) the global norm computed after the overall update reads

$$\|\boldsymbol{R}^{\text{glob}}_{\text{GPA}}[\boldsymbol{F}_{n,k}, \boldsymbol{K}_{n,\ell}, \Delta^{\ell}_{\boldsymbol{K}}]\| \tag{3.8}$$

$$= \|\mathfrak{P}[\boldsymbol{F}_{n,k}, \boldsymbol{K}_{n,\ell-1}] + \langle \partial_{\boldsymbol{K}_{n,\ell-1}} \mathfrak{P}[\boldsymbol{F}_{n,k}, \boldsymbol{K}_{n,\ell-1}] | \Delta_{\boldsymbol{K}} \rangle \|$$

- If the local correction $\Delta^{\ell}_{\boldsymbol{K}}$ is larger than the convergence radius of the Taylor expansion (3.8) in the local variable, the update and the global residuum check are likely to fail.
- While each local Newton step induces at least one global Newton step, each global Newton step induces at maximum one local Newton step.

Although the GPA algorithm is very potent to compute scenarios much more general e.g. than RMA (cf. [51]), the operator splitting still occassionally causes high number of iterations, which makes it comparably slow in some specific cases[1].

3.4. Bio Mechanics Basis Plasticity Algorithm. This section introduces an alternative algorithmic approach, which we will refer to as *Bio Mechanics Basis Plasticity Algorithm* (BMBPA) from now on. The key idea is to solve Equations (2.6a) and (2.6b) in a fully implicit way in the form of a *nested Newton iteration* [60].

To that end, assume that $\mathfrak{G}$ in Equation (2.6b) satisfies the requirements of the implicit function theorem. Then, the relation

$$\mathbf{0} = \mathfrak{G}[\boldsymbol{F}, \boldsymbol{K}] \tag{3.9}$$

in Equation (2.6b) implicitly defines the local variable $\boldsymbol{K}$ as a function of the global variable $\boldsymbol{F}$, i.e.,

$$\boldsymbol{K} = \hat{\boldsymbol{K}}(\boldsymbol{F}). \tag{3.10}$$

The function $\hat{\boldsymbol{K}}$ is called *resolution function* of the nested Newton algorithm [60]. With this notation, Equation (2.6) may equivalently be expressed as a *single* equation in the unknown $\boldsymbol{F}$, i.e.

$$0 = \mathfrak{P}[\boldsymbol{F}, \hat{\boldsymbol{K}}(\boldsymbol{F})] = \hat{\mathfrak{P}}[\boldsymbol{F}], \tag{3.11}$$

where the Jacobian functional of $\hat{\mathfrak{P}}$ is given by

$$D_{\boldsymbol{F}} \hat{\mathfrak{P}}[\boldsymbol{F}] = \partial_{\boldsymbol{F}} \mathfrak{P}[\boldsymbol{F}, \hat{\boldsymbol{K}}(\boldsymbol{F})] + \partial_{\boldsymbol{K}} \mathfrak{P}[\boldsymbol{F}, \hat{\boldsymbol{K}}(\boldsymbol{F})] . D_{\boldsymbol{F}} \hat{\boldsymbol{K}}(\boldsymbol{F}). \tag{3.12}$$

The unknown term $D_{\boldsymbol{F}} \hat{\boldsymbol{K}}(\boldsymbol{F})$ can be obtained by the implicit function theorem: Starting from the identity

$$\mathbb{O} \overset{!}{=} D_{\boldsymbol{F}} \hat{\mathfrak{G}}[\boldsymbol{F}] = \partial_{\boldsymbol{F}} \mathfrak{G}[\boldsymbol{F}, \hat{\boldsymbol{K}}(\boldsymbol{F})] + \partial_{\boldsymbol{K}} \mathfrak{G}[\boldsymbol{F}, \hat{\boldsymbol{K}}(\boldsymbol{F})] : D_{\boldsymbol{F}} \hat{\boldsymbol{K}}(\boldsymbol{F}),$$

where $\mathbb{O}$ denotes the fourth-order null tensor, we exploit that $\partial_{\boldsymbol{K}} \hat{\mathfrak{G}}[\boldsymbol{F}, \hat{\boldsymbol{K}}(\boldsymbol{F})]$ is an invertible fourth-order tensor, and obtain

$$D_{\boldsymbol{F}} \hat{\boldsymbol{K}}(\boldsymbol{F}) = -(\partial_{\boldsymbol{K}} \mathfrak{G}[\boldsymbol{F}, \hat{\boldsymbol{K}}(\boldsymbol{F})])^{-1} : \partial_{\boldsymbol{F}} \mathfrak{G}[\boldsymbol{F}, \hat{\boldsymbol{K}}(\boldsymbol{F})].$$

[1] When we applied the classical GPA to the mathematical model presented in Section 4 to simulate 30 percentage of the deformation imposed to a cubic domain, it was not possible to come to an end of the computations within a reasonable time, moreover it took several months to finalize a single computation at the medium sized GCSC Cesari cluster using 80 processes. Indeed, the model refers to the one phase case of the anisotropic tissue model published in [19] and is presented in detail in Appendix A.

We call $D_{\boldsymbol{F}}\hat{\mathfrak{P}}[\boldsymbol{F}]$ *global Jacobian functional* and $\partial_{\boldsymbol{K}}\hat{\mathfrak{G}}[\boldsymbol{F},\hat{\boldsymbol{K}}(\boldsymbol{F})]$ *local Jacobian*. This allows to recast Equation (3.12) in the form

$$D_{\boldsymbol{F}}\hat{\mathfrak{P}}[\boldsymbol{F}] = \partial_{\boldsymbol{F}}\mathfrak{P}[\boldsymbol{F},\hat{\boldsymbol{K}}(\boldsymbol{F})] - \partial_{\boldsymbol{K}}\mathfrak{P}[\boldsymbol{F},\hat{\boldsymbol{K}}(\boldsymbol{F})].\{\partial_{\boldsymbol{K}}\hat{\mathfrak{G}}[\boldsymbol{F},\hat{\boldsymbol{K}}(\boldsymbol{F})])^{-1} : \partial_{\boldsymbol{F}}\mathfrak{G}[\boldsymbol{F},\hat{\boldsymbol{K}}(\boldsymbol{F})]\}.$$

We now cast the BMBPA procedure as a Newton method in two steps.

3.4.1. *Solution of the global system.* The linearization of $\hat{\mathfrak{P}}$ from (3.11) in a neighborhood of $\boldsymbol{F}$ using an increment $\Delta_{\boldsymbol{F}}$ yields

$$0 = \hat{\mathfrak{P}}(\boldsymbol{F}+\Delta_{\boldsymbol{F}}) = \hat{\mathfrak{P}}(\boldsymbol{F}) + \langle D_{\boldsymbol{F}}\hat{\mathfrak{P}}[\boldsymbol{F}]|\Delta_{\boldsymbol{F}}\rangle + o(\|\Delta_{\boldsymbol{F}}\|), \quad \|\Delta_{\boldsymbol{F}}\| \to 0. \tag{3.13}$$

Each Newton iteration for computing an increment $\Delta_{\boldsymbol{F}}$ of the global variable $\boldsymbol{F}$ is thus given by

$$\left\langle J^{\text{glob}}_{\text{BMBPA}}[\boldsymbol{F},\hat{\boldsymbol{K}}(\boldsymbol{F})]|\Delta_{\boldsymbol{F}}\right\rangle = -R^{\text{glob}}_{\text{BMBPA}}[\boldsymbol{F},\hat{\boldsymbol{K}}(\boldsymbol{F})], \tag{3.14a}$$

where

$$J^{\text{glob}}_{\text{BMBPA}}[\boldsymbol{F},\hat{\boldsymbol{K}}(\boldsymbol{F})] := D_{\boldsymbol{F}}\hat{\mathfrak{P}}[\boldsymbol{F}], \tag{3.14b}$$

$$R^{\text{glob}}_{\text{BMBPA}}(\boldsymbol{F},\boldsymbol{K}(\boldsymbol{F})) := \hat{\mathfrak{P}}(\boldsymbol{F},\hat{\boldsymbol{K}}(\boldsymbol{F})). \tag{3.14c}$$

3.4.2. *Solution of the local system.* Due to the implicit dependency of $\hat{\boldsymbol{K}}$ on $\boldsymbol{F}$, the local variables $\hat{\boldsymbol{K}}$ must be updated as well. To that end, consider (3.9): For a given value of $\boldsymbol{F}$, a Taylor expansion of $\hat{\mathfrak{G}}$ only with respect to $\boldsymbol{K}$ yields

$$0 = \mathfrak{G}[\boldsymbol{F},\boldsymbol{K}+\Delta_{\boldsymbol{K}}] = \mathfrak{G}[\boldsymbol{F},\boldsymbol{K}]+\partial_{\boldsymbol{K}}\mathfrak{G}[\boldsymbol{F},\boldsymbol{K}] : \Delta_{\boldsymbol{K}} + o(\|\Delta_{\boldsymbol{K}}\|),\ \|\Delta_{\boldsymbol{K}}\| \to 0. \tag{3.15}$$

To compute $\Delta_{\boldsymbol{K}}$ for one Newton step, we have to solve

$$\mathbb{J}^{\text{loc}}_{\text{BMBPA}}[\boldsymbol{F},\boldsymbol{K}] : \Delta_{\boldsymbol{K}} = -\boldsymbol{R}^{\text{loc}}_{\text{BMBPA}}[\boldsymbol{F},\boldsymbol{K}], \tag{3.16a}$$

with

$$\mathbb{J}^{\text{loc}}_{\text{BMBPA}}[\boldsymbol{F},\boldsymbol{K}] = \partial_{\boldsymbol{K}}\mathfrak{G}[\boldsymbol{F},\boldsymbol{K}], \tag{3.16b}$$

$$\boldsymbol{R}^{\text{loc}}_{\text{BMBPA}}[\boldsymbol{F},\boldsymbol{K}] = \mathfrak{G}[\boldsymbol{F},\boldsymbol{K}]. \tag{3.16c}$$

3.4.3. *Algorithm 2: BMBPA.* These preliminaries allow to describe the full algorithm: Given a deformation gradient tensor $\boldsymbol{F}_0$, we obtain the corresponding remodeling tensor $\boldsymbol{K}_0 = \hat{\boldsymbol{K}}(\boldsymbol{F}_0)$. All following steps can be computed by a "nested" Newton method [60]: In an outer enclosing loop, which we refer to as "global" Newton method, we use (3.14a) to obtain an update $\Delta_{\boldsymbol{F}}$ of the deformation tensor, i.e.

$$\boldsymbol{F} = \boldsymbol{F}_0 + \Delta_{\boldsymbol{F}}.$$

With this value of $\boldsymbol{F}$, we need to resolve the nonlinear Equation (3.9), in order to compute the resolution function (3.10). This is achieved in an inner Newton iteration cycle, which we refer to as "local" Newton method. This method is based on computing updates $\Delta_{\boldsymbol{K}}$ using (3.16a). Algorithm 2 provides details on the BMBPA, in particular on the sub-structure and ordering of the Newton steps.

Algorithm 2 BMBPA algorithm for one single time step with the focus upon the nested Newton procedure, assuming that the result of the former time step $\boldsymbol{F}_{n-1}$ (and $\boldsymbol{K}_{n-1}(\boldsymbol{F}_{n-1})$) is known (as initial value in case that $n = 1$ or computed for the case $n > 1$ with the given algorithm). In particular, while each global Newton step induces at least one local Newton step, each local Newton step induces at maximum one global Newton step, in exact opposite to the GPA case.

1: $k = 1$, $\boldsymbol{F}_{n,k-1} = \boldsymbol{F}_{n-1}$, $\boldsymbol{K}(\boldsymbol{F}_{n,k-1}) = \boldsymbol{K}(\boldsymbol{F}_{n-1})$ ▷ start time step, assign initial values
2: **if** $R^{\text{glob}} = \|\boldsymbol{R}^{\text{glob}}_{\text{BMBPA}}[\boldsymbol{F}_{n,k-1}, \boldsymbol{K}(\boldsymbol{F}_{n,k-1})]\| > \epsilon_G$ **then** ▷ global residuum (3.14c) not converged
3: $< J^{\text{glob}}_{\text{BMBPA}}[\boldsymbol{F}_{n,k-1}, \boldsymbol{K}(\boldsymbol{F}_{n,k-1})] | \Delta^k_{\boldsymbol{F}} >= -R^{\text{glob}}_{\text{BMBPA}}(\boldsymbol{F}_{n,k-1}, \boldsymbol{K}(\boldsymbol{F}_{n,k-1}))$ ▷ solve for $\Delta^k_{\boldsymbol{F}}$ by inverting the system
4: $\boldsymbol{F}_{n,k} = \boldsymbol{F}_{n,k-1} + \Delta^k_{\boldsymbol{F}}$ ▷ global Newton step-accept
5: $\ell = 1$, $\boldsymbol{K}_{n,\ell-1} = \boldsymbol{K}(\boldsymbol{F}_{n,k-1})$ ▷ initial value for local Newton unknown
6: **if** $R_{\text{loc}} = \|\boldsymbol{R}^{\text{loc}}_{\text{BMBPA}}[\boldsymbol{F}_{n,k}, \boldsymbol{K}_{n,\ell-1}]\| > \epsilon_L$ **then** ▷ local residuum (3.16c) not converged
7: $[\mathbb{J}^{\text{loc}}_{\text{BMBPA}}[\boldsymbol{F}_{n,k}, \boldsymbol{K}_{n,\ell-1}]]\Delta^\ell_{\boldsymbol{K}} = -\boldsymbol{R}^{\text{loc}}_{\text{BMBPA}}[\boldsymbol{F}_{n,k}, \boldsymbol{K}_{n,\ell-1}]$ ▷ Solve local system (3.16a), solve for $\Delta^\ell_{\boldsymbol{K}}$ with final $\boldsymbol{F}_{n,k}$
8: $\boldsymbol{K}_{n,\ell} = \boldsymbol{K}_{n,\ell-1} + \Delta^\ell_{\boldsymbol{K}}$ ▷ local Newton step-accept
9: $\ell = \ell + 1$, **go to** 6 ▷ start new *local* Newton round
10: **else** ▷ local residdum converged, $R_{\text{loc}} < \epsilon_L$
11: $\boldsymbol{K}(\boldsymbol{F}_{n,k}) = \boldsymbol{K}_{n,\ell-1}$, $k = k + 1$, **go to** 2 ▷ start next *global* Newton round
12: **end if** ▷ local Newton finished
13: **else** ▷ global residuum converged, $R_{\text{glob}} < \epsilon_G$
14: $\boldsymbol{F}_n = \boldsymbol{F}_{n,k}$, $\boldsymbol{K}_n = \boldsymbol{K}(\boldsymbol{F}_{n,k})$, $n = n + 1$, **go to** 1 ▷ time step finished
15: **end if** ▷ global Newton finished

3.4.4. *Features of the BMBPA.* The key features are as follows:

- The BMBPA is a *nested* Newton and *fully implicit*. The global Newton algorithm is enclosing the local Newton algorithm. The local problem is solved *completely*[2] in the inner loop, *for each* update of the global variable in the outer loop. This is due to the fact that we consider the local variables simply to be a function of the global ones.
- The global residuum that is checked after each nested Newton step (which includes a single global Newton and as many local Newton steps as neccessary) has the following value:

[2] This means that we perform as many local Newton steps as needed to pass below the given threshold for the local residuum (using the updated global and local values), before evaluating if another global Newton step is necessary. In particular, the global residuum checked after the global update inserts both, local and global variables, in an updated manner.

$$\begin{aligned}(3.17)\quad &\|\boldsymbol{R}^{\mathrm{glob,up}}_{\mathrm{BMBPA}}(\boldsymbol{F}_{n,k}, \boldsymbol{K}(\boldsymbol{F}_{n,k}))\| \\ &\qquad = \|\mathfrak{P}^{\mathrm{glob}}_{\mathrm{BMBPA}}(\boldsymbol{F}_{n,k}, \boldsymbol{K}(\boldsymbol{F}_{n,k}))\| \\ &\qquad\quad \approx \|\mathfrak{P}^{\mathrm{glob}}_{\mathrm{BMBPA}}(\boldsymbol{F}_{n,k}, \boldsymbol{K}(\boldsymbol{F}_{n,k-1}) + \Delta_{\boldsymbol{K}}(\boldsymbol{F}_{n,k-1}))\|\end{aligned}$$

Equality in the last step of Equation (3.17) holds, iff exactly one local and one global Newton step are performed.

- Given $\boldsymbol{F}$, the local flow rule ODEs do not contain spatial couplings. Therefore, at each integration point of the grid, the local equations can be solved independently in parallel. No communication between the processors is required, which provides optimal weak and strong scalability.

As a next step, both algorithms can be compared.

3.5. Comparison of GPA and BMBPA. As stated in (3.3) and (3.16a) respectively, a single Newton step for the local problem is identical for GPA and BMBPA. This is consistent with the derivation in (3.15). There are, however, differences with respect to the ordering of global and local Newton steps and the convergence criteria, in particular w.r.t. the residual of the global problem.

TABLE 1. Summary of key properties of GPA and BMBPA.

Property	GPA	BMBPA
Implicit Function theorem	no	yes
"Visible" variables	$\boldsymbol{F}$ and $\boldsymbol{K}$	$\boldsymbol{F}$
"Invisible" variables	—	$\boldsymbol{K} \equiv \hat{\boldsymbol{K}}(\boldsymbol{F})$
Newton enclosing systems	local encloses global	global encloses local
Outer Newton	local system	global system
Inner Newton	global system	local system
Global Taylor expansion in	total: $\boldsymbol{F}$; partial: $\boldsymbol{K}$	total: $\boldsymbol{F}$
Local Taylor expansion in	partial: $\boldsymbol{K}$	partial: $\boldsymbol{K}$
Global residuum	redefined	standard form
Local residuum	standard form	standard form
Fully global residuum check	no	yes
Fully local residuum check	yes	yes
line search global	yes	yes
line search local	yes (originally no [51])	yes
# global vs. local steps	# global $\geqslant$ # local	# local $\geqslant$ # global
parallel scalability local Newton	very bad	optimal
operator splitting	yes	no
Increment order global Newton	in part 1, in part 2	unique 1
Increment order local Newton	unique 1	unique 1
Nested Newton	no	yes
monolithic	no	yes
Fully implicit	no	yes

3.5.1. *Ordering of global and local steps.* The BMBPA performs as many local Newton steps as required for local convergence. The global convergence is then considered in an outer loop. For the classic GPA, each single local Newton step is followed by as many global Newton steps as needed to reach global convergence.

3.5.2. *Taylor expansion of global residual.* The original intention of the GPA [51] was to perform at first the Taylor expansion with respect to the local variable $\boldsymbol{K}$ using the partial differentiation, and to use this expression as basis for the Taylor expansion with respect to the global variable $\boldsymbol{F}$ using the total differentiation. One consequence of the mixed Taylor expansion is that the orders of the increments which are taken into account are not unique: In part, this resulted in some increment orders of the magnitude one, while others are of effective order two[3]. The incorporation of terms of second order is specific for the GPA global Newton method.

In retrospective, in case of the GPA, the computation of the global variable update (3.5) can be understood as solution of the global system (2.6a) based upon the Taylor expansion of the global system by means of the total derivation with respect to the global variable $\boldsymbol{F}$, and the partial derivation with respect to the local variable $\boldsymbol{K}$. This indicates that, to some extent, the two unknowns are treated in a similar, but not equal way. The GPA specific double Taylor expansion can be interpreted as[4]

$$
\begin{aligned}
&\mathfrak{P}[\,\boldsymbol{F}+\Delta_{\boldsymbol{F}},\boldsymbol{K}+\Delta_{\boldsymbol{K}}]\\
&\quad\approx \mathfrak{P}[\boldsymbol{F},\boldsymbol{K}]+\langle D_{\boldsymbol{F}}\mathfrak{P}[\boldsymbol{F},\boldsymbol{K}]|\Delta_{\boldsymbol{F}}\rangle+\langle\partial_{\boldsymbol{K}}\mathfrak{P}[\boldsymbol{F},\boldsymbol{K}]|\boldsymbol{\Delta}_{\boldsymbol{K}}\rangle+\underbrace{\mathcal{A}(\Delta_{\boldsymbol{F}}\Delta_{\boldsymbol{K}})}_{\text{second order in increments}}\\
&\quad\approx \mathfrak{P}[\boldsymbol{F},\boldsymbol{K}]+\langle[\partial_{\boldsymbol{F}}\mathfrak{P}[\boldsymbol{F},\boldsymbol{K}]+\partial_{\boldsymbol{K}}\mathfrak{P}[\boldsymbol{F},\boldsymbol{K}].D_{\boldsymbol{F}}\,\boldsymbol{K}]|\Delta_{\boldsymbol{F}}\rangle+\langle\partial_{\boldsymbol{K}}\mathfrak{P}[\boldsymbol{F},\boldsymbol{K}]|\boldsymbol{\Delta}_{\boldsymbol{K}}\rangle\\
&\quad= \mathfrak{P}[\boldsymbol{F},\boldsymbol{K}]+\langle[\partial_{\boldsymbol{F}}\mathfrak{P}[\boldsymbol{F},\boldsymbol{K}]-\partial_{\boldsymbol{K}}\mathfrak{P}[\boldsymbol{F},\boldsymbol{K}].(\partial_{\boldsymbol{K}}\mathfrak{G}[\boldsymbol{F},\boldsymbol{K}])^{-1}:\partial_{\boldsymbol{F}}\mathfrak{G}[\boldsymbol{F},\boldsymbol{K}]]|\Delta_{\boldsymbol{F}}\rangle\\
&\qquad+\langle\partial_{\boldsymbol{K}}\mathfrak{P}[\boldsymbol{F},\boldsymbol{K}]|\boldsymbol{\Delta}_{\boldsymbol{K}}\rangle
\end{aligned}
$$

where in the third, fourth and fifth line $\boldsymbol{K}$ is understood as $\hat{\boldsymbol{K}}(\boldsymbol{F})$. A reordering of this expression yields global GPA Jacobian and global GPA residuum, cf. (3.5) and (3.6).

In case of the BMBPA, the global system is solved purely on the basis of the classical type of Taylor expansion with respect to the variable $\boldsymbol{F}$ only (3.13) leading to the global variable update (3.14a). As usual in classical Newton procedures, the Taylor expansion is incorporating namely, simply and only the first order contribution of the increment of the global variable $\boldsymbol{F}$, i.e. unique $\Delta_{\boldsymbol{F}}$.

---

[3] We have order one for the expansion in the pure variables $\boldsymbol{F}$ and $\boldsymbol{K}$, i.e. $\boldsymbol{\Delta}_{\boldsymbol{F}}$ and $\boldsymbol{\Delta}_{\boldsymbol{K}}$, but effectively order two for the mixing of the expansion originating from mixtures of the expansion in both variables, resulting in terms of type "$\Delta_{\boldsymbol{F}}\Delta_{\boldsymbol{K}}$" (product to be understood heuristically). This means that the GPA accounts for terms of type "$\Delta_{\boldsymbol{F}}\Delta_{\boldsymbol{K}}$", but not of type "$\Delta^2_{\boldsymbol{F}}$" nor "$\Delta^2_{\boldsymbol{K}}$".

[4] To facilitate reading and principal insight, in this expression, except for the second line where we noted the heuristic functional $\mathcal{A}(\Delta_{\boldsymbol{F}}\Delta_{\boldsymbol{K}})$ which symbolizes the contribution "linear" in the heuristic expression $\Delta_{\boldsymbol{F}}\Delta_{\boldsymbol{K}}$, we did not explicitly write the terms of second order which in fact nevertheless in part contribute to the GPA system. Except for the second line, we neglect $\mathcal{A}(\Delta_{\boldsymbol{F}}\Delta_{\boldsymbol{K}})$ in the reformulation to facilitate reading and catching the major points.

3.5.3. *Global system.* The global Jacobian functional is identical[5] for both GPA, see Equation (3.6a), and BMBPA, see Equation (3.14a), and involves in both cases the total differentiation w.r.t the global variable $\boldsymbol{F}$. The residuals (3.6c) and (3.14c) are different.

While the global residual (3.14c) in the BMBPA is defined in classic form, the residual (3.6c) for the GPA is derived from a Taylor expansion. It includes an additional term, which corresponds to the changes induced by the tentative update of the local variables. As a result, both approaches yield different results. However, note that (3.6c) is still consistent and yields a convergent method for $\|\Delta_{\boldsymbol{K}}\| \to 0$. Finally, we note that even in case in which we assume that only one local and one global Newton steps are applied, the residuals are different:

$$\underbrace{\|\mathfrak{P}(\boldsymbol{F}_{n,k}, \boldsymbol{K}(\boldsymbol{F}_{n,k-1}) + \Delta_{\boldsymbol{K}}(\boldsymbol{F}_{n,k-1}))\|}_{\text{BMBPA residual}}$$

$$\overset{\text{in gen.}}{\neq} \underbrace{\|\mathfrak{P}(\boldsymbol{F}_{n,k}, \boldsymbol{K}_{n,\ell-1}) + \partial_{\boldsymbol{K}_{n,\ell-1}}\mathfrak{P}(\boldsymbol{F}_{n,k}, \boldsymbol{K}_{n,\ell-1}) \cdot \Delta_{\boldsymbol{K}}\|}_{\text{GPA residual}}$$

The effect of this behavior is even more pronounced, as for the GPA, the global residual is never checked for entirely updated local variables. In contrast, the BMBPA provides a full check after each update.

3.5.4. *Line search.* For the sake of simplicity, a line search strategy is not included in algorithms 1 and 2 respectively. However, in practice a line search globalization is used in both Newton procedures. In its original version, the GPA was without line search in the local Newton [51], but was added in the course of this project.

3.5.5. *Summary.* Table 1 summarizes the key properties of GPA and BMBPA. The BMBPA is fully implicit: The crucial difference is that in the case of the BMBPA, formally, for the global Newton the local system does not exist, but is incorporated in the resolution function, i.e. in the dependency of the local variables on the global ones. In principle, the local variables can always be computed on the basis of the global variables, without further knowledge. However, in the practical case, the local Newton would never terminate without knowledge of the former local variables as start values.

To conclude, for the classical GPA, the global Newton is nested within a local Newton, whereas for the BMBPA, the local Newton is nested within a global Newton procedure. Hence, for the classical GPA, the number of local Newton steps is a lower bound for the global Newton steps, whereas for the BMBPA, the number of local Newton steps is an upper bound for the global Newton steps. For parallelization purposes, the BMBPA is thus much better suited, as local Newton steps can be performed with perfect parallel performance.

[5] This identity is valid except for terms of second order in the increments as indicated before. In fact, the aforementioned term $\mathcal{A}(\Delta_{\boldsymbol{F}}\Delta_{\boldsymbol{K}})$, i.e. of second order in the increments, contributes to the GPA global Jacobian part. In contrast, as usual in classical Newton procedures, increments do not form part of the global BMBPA Jacobian operator at all.

4. Description of numerical experiments

In this section, we discuss about the space and time discretizations of the model equations (2.7a) and (2.7b) (FE in space and implicit Euler in time) and the resolution of the considered tissue's anisotropy, we introduce the computational domains used for the numerical experiments and, for each of them, we analyse the number of degrees of freedom (DoF). Finally, we describe the applied solvers.

In order to account for the concrete form of the model equations (2.7a) and (2.7b) which define the basis of the numerical experiments, we collect in Appendix A all the details concerning the constitutive description of the tissue's mechanical properties and anisotropy.

Space and time discretization. In our framework, Equation (2.7a), representing the weak form of the balance of linear momentum, is discretized by means of Finite Elements of first order [59], while Equation (2.7b), representing the remodeling law, is discretized with an implicit Euler time stepping method of first order. Indeed, since no spatial derivative of $\boldsymbol{K}$ appears in Equation (2.7b), no spatial discretization of it is needed, so that it is sufficient to evaluate Equation (2.7b) at the integration points of the Finite Elements.

We discretize the time window $\mathscr{I}$ over which the evolution of the system is monitored into N intervals of the type $[t_{n-1}, t_n]$, with $n \in \mathbb{N}, n \geqslant 1$, and such that $t_n = t_{n-1} + \Delta t_n$, with Δt_n being the nth time step. Finally, for every function $\mathcal{F}\colon \mathscr{B} \times \mathscr{I} \to \mathscr{V}$ taking values in the vector space $\mathscr{V}$, we set $\mathcal{F}_n(X) := \mathcal{F}(X, t_n)$, for every $X \in \mathscr{B}$ and $t_n \in \mathscr{I}$. Hence, the discretized version of Equations (2.7a) and (2.7b) can be put in the form

$$\int_{\mathscr{B}} \hat{\boldsymbol{P}} \circ (\boldsymbol{F}_n, \boldsymbol{K}_n) : \mathfrak{g}\mathrm{Grad}\tilde{\boldsymbol{v}} = 0, \tag{4.1a}$$

$$2\Delta t_n \mathcal{T} \circ (\boldsymbol{F}_n, \boldsymbol{K}_n, \dot{\boldsymbol{K}}_n) + 2\Delta t_n [\zeta \circ (\boldsymbol{F}_n, \boldsymbol{K}_n)][\boldsymbol{M} \circ (\boldsymbol{F}_n, \boldsymbol{K}_n)] = \boldsymbol{0}, \tag{4.1b}$$

with $\boldsymbol{F}_n = D\chi_n$ and $\mathcal{T} \circ (\boldsymbol{F}_n, \boldsymbol{K}_n, \dot{\boldsymbol{K}}_n) = \mathrm{sym}(\dot{\boldsymbol{K}}_n \boldsymbol{K}_n^{-1} \boldsymbol{C}_n^{-1})$. By introducing the time discrete counterpart of $\dot{\boldsymbol{K}}_n$ as $\dot{\boldsymbol{K}}_n = (\boldsymbol{K}_n - \boldsymbol{K}_{n-1})/\Delta t_n$, we have

$$\begin{aligned} 2\Delta t_n \mathcal{T} \circ (\boldsymbol{F}_n, \boldsymbol{K}_n, \dot{\boldsymbol{K}}_n) &= 2\Delta t_n \check{\mathcal{T}} \circ (\boldsymbol{F}_n, \boldsymbol{K}_n, \boldsymbol{K}_{n-1}) \\ &= (\boldsymbol{K}_n - \boldsymbol{K}_{n-1})\, \boldsymbol{K}_n^{-1} \boldsymbol{C}_n^{-1} + \boldsymbol{C}_n^{-1} \boldsymbol{K}_n^{-\mathrm{T}} (\boldsymbol{K}_n^{\mathrm{T}} - \boldsymbol{K}_{n-1}^{\mathrm{T}}). \end{aligned}$$

Finally, we provide the spatial discretization of Equation (4.1a) by considering a regular triangularization $\mathscr{T}$ (including the possibility of unstructured grids) of the closure of $\mathscr{B}$ in N_h non overlapping elements, defining a grid with characteristic length h and introducing the space of polynomials $\mathbb{P}_1(T_i)$ of order 1 and associated with the ith element of the triangularization $\mathscr{T}$, with $i = 1, \cdots, N_h$.

Directional average. To account for the statistical orientation of the fibers, we employ the directional averages introduced by Lanir [65] and adopted in [29–34, 46], in contexts analogous to the present one, i.e.

$$\langle\!\langle f_X \rangle\!\rangle = \int_0^{2\pi} \int_0^{\pi} \hat{f}_X(\theta, \varphi) \hat{\mathcal{F}}(\theta) \sin\theta \, \mathrm{d}\theta \, \mathrm{d}\varphi, \tag{4.2}$$

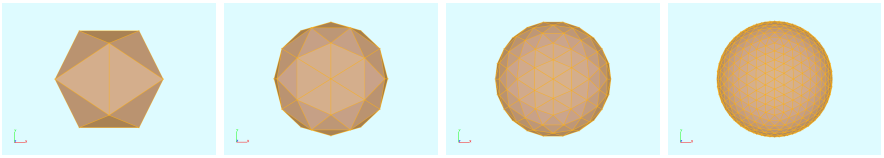

FIGURE 1. Refinement of the triangularized descrete representation of the unit sphere by means of ProMesh [80, 82] emloyed for the numerical computation of directional averages through the Graphical Spherical Design Algorithm. Sphere refinement levels 0-3.

to indicate the directional average of a quantity of interest depending on the fiber distribution (all the details are reported in Appendix A), where $\mathcal{F}$ is the probability density function associated with the statistical distribution of fibers. In other words, Equation (4.2) express the integration of a (scalar, vector or tensor) function f, depending on the local direction of fiber alignment, over the unit sphere.

The numerical integration of Equation (4.2) is performed by having recourse to the *Graphical Spherical Design Algorithm* (GSDA). Accordingly, we use a discretized (triangulated) version of the unit sphere as basis for the integration points, corresponding to the centers of the triangles of the discrete representation of the sphere, while the surfaces of the triangles correspond to surface measures. The surface triangulation is performed with ProMesh [80, 82]. We remark that, this kind of surface integration allows, in principle, for arbitrary precision of the integration, given sufficiently fine refinement levels of the surface. Figure 1 displays graphically the triangulated unit sphere at different refinement levels.

Note that whereas the Spherical Design Algorithm (SDA) [35], employed in other works studying fiber-reinforced biological tissues [11], call for an integration over a very small subset of integration points chosen with specific techniques, the massively parallel environment which we apply in this study allows for much more evaluation points of the spatial integral over the sphere. In this paper, we use a simple mid point integration rule of the triangles discretizing the sphere, which we refine step-wise to test for convergence and robustness of the results. In future projects, one might take into account further improvements of the GSDA (such as specific weights and higher integration orders at the single triangles of the discretized sphere) to allow for more efficient *and* more precise evaluations. However, this task is not subject of this study presented here.

By introducing a triangularized discrete representation of the unit sphere, denoted by $\mathscr{U}$ and containing M triangles, we approximate Equation (4.2) as

$$\langle\langle f_X \rangle\rangle \approx \sum_{i=1}^{M} \frac{\mathcal{S}_i}{\pi} \hat{f}_X(\theta_i, \varphi_i)\mathcal{F}(\theta_i),$$

with (θ_i, φ_i) individuating the center of the ith triangle and with $\mathcal{S}_i$ denoting its surface measure.

Test cases: geometries, boundary and initial conditions, DoFs. For our computations, we use two different 3D computational domains and, for each of them, we consider specific benchmark tests: shear-compression test of a cubic domain and an unconfined compression test for a cylindrical domain in displacement control. In both cases, the external load are applied in terms of Dirichlet conditions. Moreover, loads are applied linearly increasing with time by means of a linear increasing load ramp, such that at the final time, the full load is reached. In all the cases, we compare the isotropic with the anisotropic model of remodeling.

The degrees of freedom are computed as the sum of the global degrees of freedom (DoFs) (vertex number times three, as three components correspond to the global unknown χ), plus the local DoFs, which are computed as the number of integration points (IPs) per element (the number of IPs depends on the chosen quadrature order) times the number of elements of the computational elements of the Finite Element mesh times the nine components of the remodeling tensor. For all computations, we use Finite Elements of quadrature order one.

Test case one: shear compression test of a cubic domain. The cube has side length $L = 1$ cm and it is discretized by means of hexahedral elements. This means that, for integration order one, each hexahedral element contains 8 integration points. Therefore, in order to compute the number of local DoFs, one has to multiply the number of elements in the case of the cube by 72. Hence, we have

lev	glob. DoFs	#elem	loc. Dofs
3	14,739	4,096	294,912
4	107,811	32,768	7,762,392
5	823,875	262,144	18,874,368

In this case, we perform a shear-compression test, which means that we enforce Dirichlet conditions such that the upper side of the cube is sheared in x direction up to 30% and experiences a compression of 30% in y direction. The lower side is fixed with zero Dirichlet conditions while the remaining boundary is free of applied contact forces.

Test case two: unconfined compression test of a cylindrical domain. The cylinder has radius $R = 1.5$ cm and height $H = 1$ cm. The basic elements of the cylinder are prisms, as the cylinder is constructed based upon the extrusion of triangles. This means that, at integration order one, the prism elements of the cylinder contain 6 integration points each. Therefore, in order to compute the number of local DoFs, one has to multiply the number of elements with 54. In this case, we have

lev	glob. DoFs	#elem	loc. Dofs
4	931,539	589,824	31,850,496

For what concerns boundary conditions, the upper side experiences a compression of 30% in z direction. The lower side is fixed with zero Dirichlet conditions, while traction-free conditions are applied to the lateral surface of the cylinder.

Technical solution framework. All computations were implemented under the simulation software UG4 [55, 81, 90]. The linear solver of the nonlinear global Newton procedure (referring to $\boldsymbol{F}$) applies the BiCGStab method preconditioned

with an ILU, whereas the local Newton (referring to $\boldsymbol{K}$) performs the exact inversion of the dense matrix of the local Jacobian (which indeed, due to the symmetry in $\boldsymbol{K}$, is a 6×6 matrix) at each integration point. The differentiation of local and global Jacobian are performed numerically.

Computing facilities. The computations were performed all in parallel. Some computations were performed on the GCSC Cesari cluster (for a description cf. e.g. [61]) and others were performed on the HLRS Stuttgart Apollo Hawk supercomputer, cf. [54].

5. Simulation results

In this section, we discuss the peculiarities of the BMBPA and its novelties in light of the numerical results obtained by simulating the benchmark tests introduced in the previous section. Moreover, we compare the numerical solutions provided by the BMBPA with those obtained with the GPA and, for this reason, we also run numerical simulations in which we consider isotropic behavior of the considered medium, in order to have a term of comparison with other works [19,49,51]. We anticipate that the application of the GPA to the considered anisotropic tissue model effectively fails, as the computation times for a single run are in the size of several months for moderate DoF numbers when performing the computations on a parallel cluster. On the other hand, the application of the BMBPA performs the same computations much faster with the same hardware setup, within the range of hours. In turn, this evidence permits to adjust the numerical procedure in order, depending on wheter one considers isotropic and anisotropic tissue description, both for cubic and cylindrical geometry. Finally, we investigate the robustness of the results in terms of computational grid and GSDA refinement, the latter calling for the discretized representation of the unit sphere, which we use for the numerical integration of directional averages.

Isotropic model. Before considering the application of the BMBPA to the fully anisotropic model, we apply it to solve the isotropic case and we compare the results obtained with the GPA in [51]. For this reason, within the test case 1, we plot the maximum eigenvalue of the elastic Kirchhoff stress tensor $\boldsymbol{\tau}_{\mathrm{e}} = J_{\mathrm{e}}\boldsymbol{\sigma} \equiv \boldsymbol{\tau}$ at the center of the unit cube, i.e., at $X = (0.5, 0.5, 0.5)$ cm, as done in [51], computed with both the GPA and the BMBPA, and, in Figure 2, we display the comparison between the two obtained curves. We obtain a complete match between the two curves and, since this is true also for other quantities of interest (not shown in this paper for the sake of brevity), we notice that, in the isotropic case, the two algorithms exhibit no appreciable difference.

Anisotropic model. Next we compare the simulation of the model adapted from [19] and recalled in appendix A, in the case of GPA and BMBPA application. In the case of the deformation of the cube under a shear-compression test, the simulation of the compressed cube yields the picture shown in Figure 3A, and the deformed cylinder is displayed in Figure 3B.

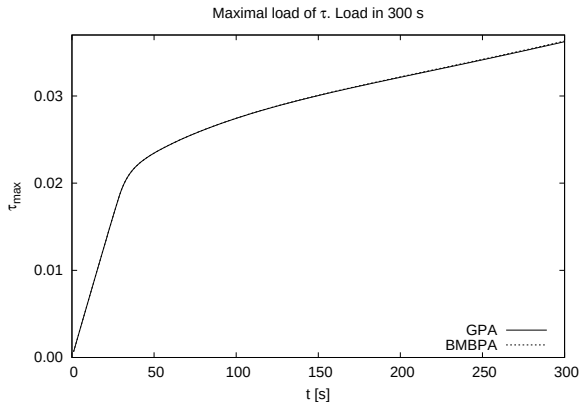

FIGURE 2. Comparison of the results obtained through the BMBPA and the GPA in the case of isotropic model of structural reorganization. We refer to [51] for a comparison with our results. The simulation results nearly coincide. Grid refinement level 4 as [51].

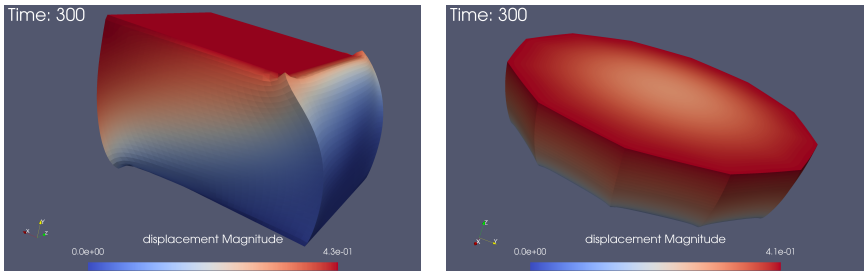

A B

FIGURE 3. Deformed geometries after 300 s of: test case 1 (shear compression of a unit cube in panel A) and test case 2 (unconfined compression test of a cylinder in panel B).

At first, we consider the results obtained with the aid of the GPA, which, in general, displayed substantial robustness issues and very long computation times, due to the property of the operator splitting method of the GPA, that the number of local Newton iterations displays a lower bound for the number of the global Newton iterations. Afterwards, we consider the aid of the new algorithm developed in this study, where the relationship between local and global Newton steps switched to its inverse compared to the GPA, making the new fully implicit BMBPA much better suitable for massively parallel computations.

Challenges in application of the classical GPA. When we tried to apply the GPA to the highly nonlinear model described in Appendix A, we were running

into substantial robustness issues. We performed the computations on our own cluster and were not limited by means of wall-time restrictions. However, even after weeks of running a single computation in parallel, we did not manage to come to an end within a reasonable computing time. The number of local and global Newton steps went so high, that the program seemed nearly to stop, despite still performing a lot of computation rounds. As the complete global Newton procedure had to be repeated for each local line search parameter in order to perform line search in the local Newton, each single local line search induced in most cases several global Newton steps. This practical example demonstrated the weaknesses of the GPA with respect to massively parallel computations. To finalize one single specific run, we needed nearly 3 months using 80 processes. Therefore, we could not perform additional numerical experiments with the GPA in the case of the anisotropic model.

5.1. Evaluations with the BMBPA method. Applying the same comparison technique for quantitative evaluations as in the before considered case of the study of [51] for a deformation time of 300 s, we get the results shown in Figure 4.

While the evaluation of the maximal eigenvalue of τ was useful for the case of more simple isotropic models, it seems to be not so useful for more advanced anisotropic tissue models. In particular, the results displayed in Figure 4 show only a small difference between the isotropic and the anisotropic case. Therefore, we apply an additional method of evaluation. Namely, we compute the Frobenius norm of the deviation of the plastic tensor from the metric tensor in the form

$$\mathfrak{F} = \tfrac{1}{2}[\boldsymbol{K}^{-\mathrm{T}}.\boldsymbol{K}^{-1} - \boldsymbol{G}] \tag{5.1}$$

Note that, when Equation (5.1) is written with respect to normalized vector bases, the matrix representation of the metric tensor $\boldsymbol{G}$ coincides with the unit matrix.

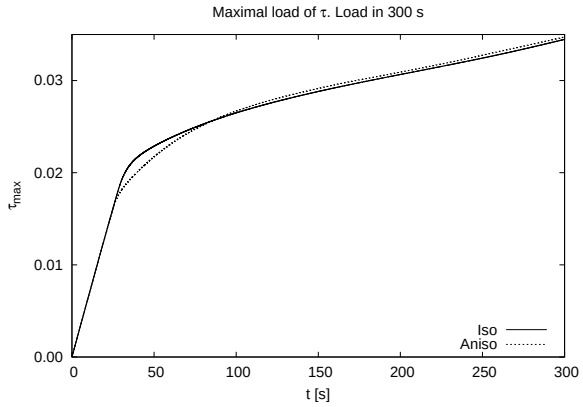

FIGURE 4. Deformation time of 300 s. BMBPA method. The evaluation refers to the maximal eigenvalue of $\boldsymbol{\tau}$ in the center of the cube. Data shown for grid refinement level 5 and GSDA level 1.

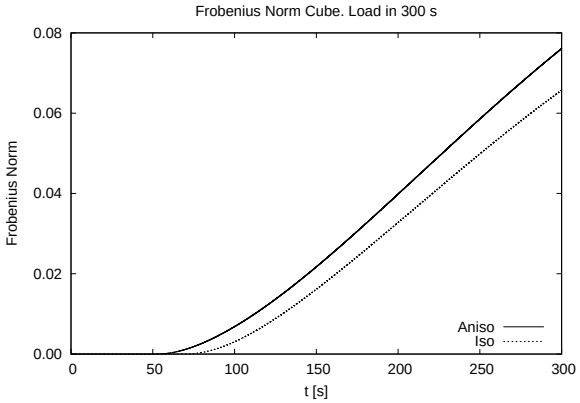

FIGURE 5. Comparison of the Frobenius Norm (5.1) of $\mathfrak{F}$ values for the isotropic and the anisotropic case for the test case one (cubic domain). Evaluations for GSDA level 2, and grid refinement level 5. Evaluation point: cf. Eq. (5.2).

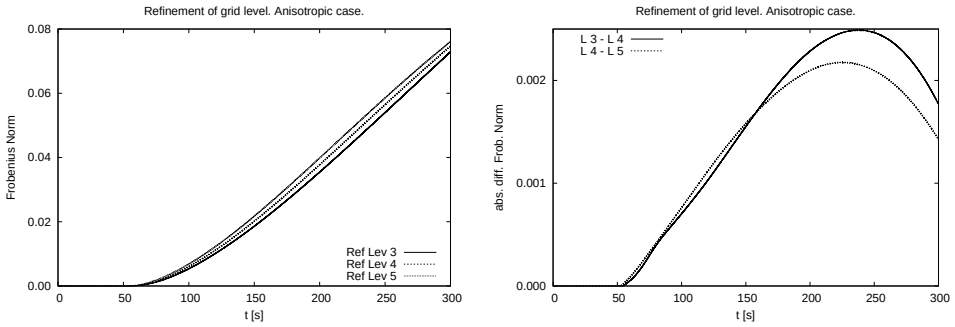

FIGURE 6. Differences for the variation of the grid refinement level (GSDA level 2) for the test case one (cubic domain). We see that with increasing grid refinement level, the results are getting more robust. Left: values; right: absolute differences.

In the case of the cube, we will perform the evaluations of $\mathfrak{F}$ at the following spatial point:

$$P_{\mathfrak{F}} = (0.9, 0.7, 0.3)\,\text{cm}. \tag{5.2}$$

Figure 5 shows the different results comparing the isotropic and anisotropic case (for refinement level 5 and GSDA level 2). Figure 6 displays the differences of the results under variation of the grid refinement level, and Figure 7 under variation of the GSDA level. With increasing GSDA level and, independently, with increasing grid refinement level, the results become more robust. Concerning the GSDA level,

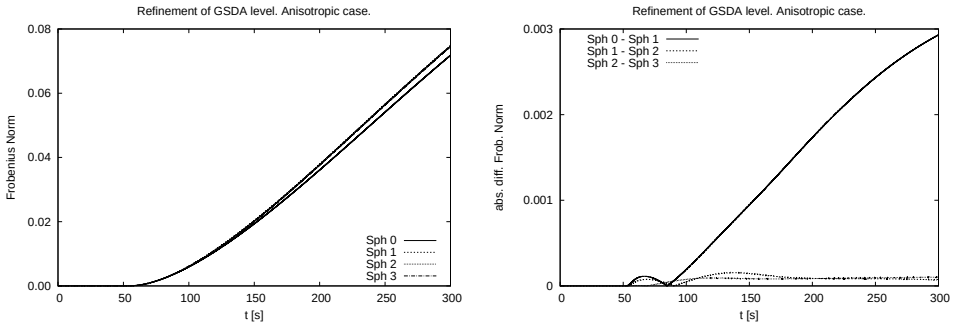

FIGURE 7. Differences for the variation of GSDA level (for refinement level 4) for the test case one (cubic domain). We see that with increasing GSDA level, the results are getting more robust. From GSDA level 1 on only very small changes. Left: values; Right: absolute differences.

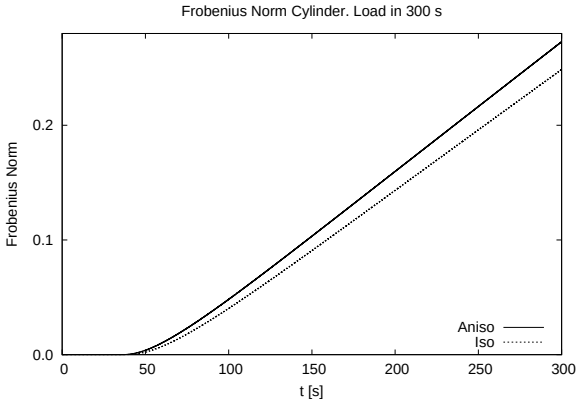

FIGURE 8. Evaluation of $\mathfrak{F}$ for the test case two (cylindrical domain) evaluated at $\boldsymbol{P}_{\mathfrak{F}}$ from Eq. (5.3).

starting from level 1, the results are already quite stable, only refinement level 0 shows major differences.

Figure 8 displays the variation of $\mathfrak{F}$ at the spatial point [19]

$$\boldsymbol{P}_{\mathfrak{F}} = (1.3, 0.0, 1.0)\,\mathrm{cm} \tag{5.3}$$

for the compressed cylinder.

5.2. Runtime comparison GPA-BMBPA. We compared the simulation times of the deformation of the cube in the anisotropic model for the GPA and the BMBPA. While the computed results agree quite well, cf. Figure 9, the real "human" simulation times needed differed strongly, cf. Figure 10. As in the case of the GPA it was not possible to come to an end of the simulation of 300 physical

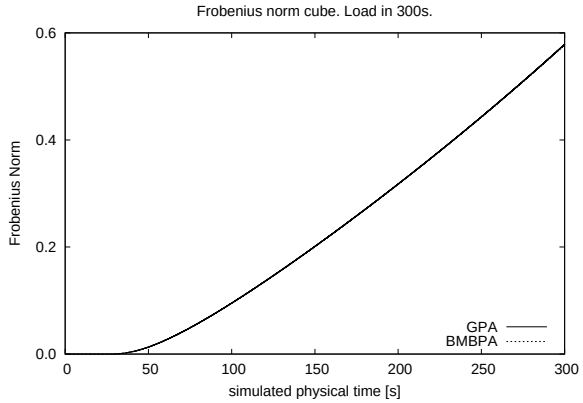

FIGURE 9. Comparison GPA vs. BMBPA Frobenius norm evaluated for the test case one (cubic domain) and evaluated at the cube center. Anisotropic tissue case. Grid refinement level 4 and GSDA level 1. GPA and BMBPA results agree very well.

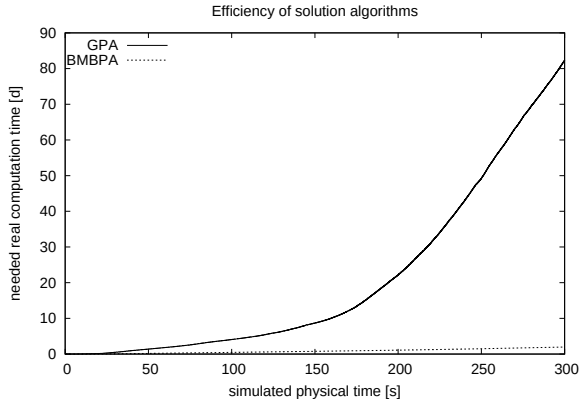

FIGURE 10. Runtime comparison to reach defined deformation for the test case one (cubic domain): GPA vs. BMBPA. Using 80 processes at GCSC Cesari cluster.

seconds (corresponding to 30 per cent deformation of the cube) within usual walltimes at modern supercomputers, we compared the runtimes exemplary at our 10 years old GCSC Cesari cluster. We used 80 processes at the GCSC Cesari cluster to compute the deformation at grid level 4 and GSDA level 1. In the case of the GPA, we needed about 12 weeks, nearly 3 months, of real / human simulation time to finalize the computations, while the full 300 physical seconds were reached in less than 2 days (47h 20min) using the BMBPA with the same refinement and hardware setup. This means that for the given configuration at moderate parallelization level with moderate DoF numbers, in this very specific case, the new algorithm is about

40 times faster. In particular, while the new algorithm permits to compute results within a reasonable "human" time, this is not possible in the case of the GPA, because a time scale of few days is definitively more efficient than one requiring up to months. We finally remark that when we were running the BMBPA for the given refinement setup using 512 processes at the present Apollo Hawk supercomputer at the HLRS Stuttgart, we needed about 5h 44min.

6. Discussion

We briefly repeat the progress of the new BMBPA algorithm and its properties compared to the GPA, and we present our next aims in this context.

We have developed a new general and efficient algorithm for elastoplastic deformations, namely for the application to biological tissue of anisotropic structure. This new algorithm allowed to perform elastoplastic deformation simulations, which the classical GPA was not able to perform in the practical case within an acceptable time. We have investigated the differences of the stress responses of isotropic and anisotropic biological tissue such as articular cartilage under elastoplastic deformations.

The BMBPA method presented in this study is based on a nested Newton method enriched by a resolution function which relates global and local variables. It combines the advantages of the classical GPA method [51], and a global fully implicit monolithic nested Newton, which has been applied for example to multiphase multicomponent flow in porous media including equilibrium reactions [60]. The major advantage of the BMBPA algorithm is that the number of local Newton steps by now is an upper bound for the number of global Newton steps, in contrast to the classical GPA. This property is of enormous importance in the context of massively parallel computations: As the local system computations are performed at each integration point completely independent of the other integration points, the local system solution is performed with perfect parallel performance.

For elastic and hyperelastic contact problems, there exist solution techniques for small strain and obstacle problems [44, 45], and more recently, also for large deformation contact problems, cf., e.g., [21, 41, 62, 91, 92]. However, to the best of our knowledge, the robust solution of problems combining contact scenarios and finite strains [21, 41, 44, 45, 57, 63, 66, 67, 75, 79, 88, 92] are limited, at most, to isotropic models.

The combination of plastic strain mechanics for large deformation problems as presented in this study might be combined with contact and obstacle problem solutions to develop approaches for large elastoplastic deformation contact problems within future projects.

7. Conclusions

This study presented the development of a novel algorithm, the BMBPA-Bio Mechanics Basis Plasticity Algorithm. The BMBPA contains all advantages of the classical semi-implicit GPA [51], but heals its disadvantages. It combines general applicability with the advantages of fully implicit approaches. The BMBPA

is an efficient fully implicit nested Newton based method to compute elastoplastic deformations of biological tissue, as it takes advantage of massively parallel supercomputer facilities. In contrast to the GPA, the BMBPA allows the evaluation of complex anisotropic material deformation scenarios within reasonable times.

Our results motivate further investigations in the field of efficient solvers of elastoplastic deformation models. Among our next aims, there is the application of the algorithm to the two-phase case. Applications of the BMBPA to other material types might be promising. It might also be interesting to test the applicability and efficacy of our new algorithm in comparison also to other plasticity algorithms in the field beyond the GPA.

In the middle run, a merging of the BMBPA with contact problem solution techniques might facilitate the evolution of realistic biophysical scenarios. Such scenarios are based upon realistic reconstructed geometries represented by unstructured grids.

In the long run, such challenging computations might allow for e.g. patient specific malignant tumor progression prediction scenarios and facilitate medical interventions.

Appendix A. Constitutive framework

This section summarizes the constitutive framework adopted in our study and taken from [19].

To measure the distribution of both the ECM and of the fibers within the tissue, we introduce the volumetric fractions

$$\varphi_{\mathrm{m}}(\cdot,t)\colon \mathscr{B}(t) \to]0,1[,$$
$$\varphi_{\mathrm{f}}(\cdot,t)\colon \mathscr{B}(t) \to]0,1[,$$

satisfying the saturation condition $\varphi_{\mathrm{m}}(x,t)+\varphi_{\mathrm{f}}(x,t)=1$, for each $x \in \mathscr{B}(t)$ and $t \in \mathscr{I}$. Moreover, differently from other works [15, 46], no active remodeling of the fibers is accounted for.

For any instant of time $t \in \mathscr{I}$, let us define the collection of the natural states associated with each material point $X \in \mathscr{B}$ as the bundle of all (relaxed tangent) spaces $\mathscr{N}_X(t)$ [19, 22], i.e.,

$$\mathscr{N}(t) := \bigsqcup_{X \in \mathscr{B}} \mathscr{N}_X(t), \text{ for all } t \in \mathscr{I}. \tag{A.1}$$

As reported in the introductory part of this paper and following [11, 15, 28, 32, 46, 50, 87], we deal with fiber-reinforced biological tissues, with the fibers oriented statistically. In particular, we can assume that the tissue is *locally transversely isotropic* at each material point $X \in \mathscr{B}$ finding itself in its natural state, thereby implying the existence of a preferred direction along which a fiber passing through X is aligned. In order to mark the local direction of alignment of a fiber in the natural state, we introduce a field of unit vectors $\mathbf{m}(\cdot,t)\colon \mathscr{B} \to \mathscr{N}(t)$, represented, in a system of spherical coordinates, as

$$\mathbf{m}(X,t) = \sin\theta\cos\phi\,\mathfrak{e}_1(X,t) + \sin\theta\sin\phi\,\mathfrak{e}_2(X,t) + \sin\phi\,\mathfrak{e}_3(X,t), \tag{A.2}$$

where $\theta \in [0, \pi]$ and $\phi \in [0, 2\pi]$ are the colatitude and the longitude, respectively. In particular, the set of all unit vectors defined in Equation (A.2) is denoted by

$$\mathbb{S}^2\mathscr{N}_X(t) = \{\mathfrak{m}_X(t) \in \mathscr{N}_X(t) : \|\mathfrak{m}_X(t)\| = 1\},$$

and it can be taken as a representation of the unit sphere centered in X. Similarly to Equation (A.1), we introduce the bundle of all directions

$$\mathbb{S}^2\mathscr{N}(t) := \bigsqcup_{X \in \mathscr{B}} \mathbb{S}^2\mathscr{N}_X(t), \text{ for all } t \in \mathscr{I}.$$

The probability density function describing the orientation of the fibers within the matrix is indicated by $\mathcal{F}\colon \mathbb{S}^2\mathscr{N}(t) \to \mathbb{R}^+$ such that $\mathcal{F}(\mathfrak{m})$ measures the probability density of finding a rectified fiber passing for $X \in \mathscr{B}$ and aligned along $\mathfrak{m}$. Finally, we introduce the structural tensor

$$\mathfrak{a} = \mathfrak{m} \otimes \mathfrak{m}, \tag{A.3a}$$

$$\boldsymbol{A} = \frac{\boldsymbol{K}\mathfrak{a}\boldsymbol{K}^{\mathrm{T}}}{(\boldsymbol{K}^{\mathrm{T}}.\boldsymbol{K}) : \mathfrak{a}}. \tag{A.3b}$$

We endow the medium under study with a strain energy density function, defined per unit volume of the natural state, given as

$$\psi_{\mathrm{R}} \equiv \psi_\nu = \varphi_{\mathrm{m}\nu}\hat{\psi}_{\mathrm{m}\nu}(\boldsymbol{C}_{\mathrm{e}}) + \varphi_{\mathrm{f}\nu}\hat{\psi}_{\mathrm{f}\nu}(\boldsymbol{C}_{\mathrm{e}}).$$

where $\varphi_{\mathrm{m}\nu}$ and $\varphi_{\mathrm{f}\nu}$ are the volumetric fractions of the matrix and of the fibers expressed per unit volume of the natural state, while $\hat{\psi}_{\mathrm{m}\nu}$ and $\hat{\psi}_{\mathrm{f}\nu}$ are the constitutive laws identifying the contributions to the overall strain energy density, ψ_ν, due to the matrix and the fibers. In particular, because of conservation of mass, both $\varphi_{\mathrm{m}\nu}$ and $\varphi_{\mathrm{f}\nu}$ are constant in time, and depend only on material points through the expression [19, 87]

$$\varphi_{\mathrm{m}\nu} = -0.062\xi^2 + 0.138\xi + 0.296,$$
$$\varphi_{\mathrm{f}\nu} = -0.062\xi^2 - 0.138\xi + 0.204,$$

with $\xi = Z/H$. We assume the matrix to be isotropic, so that $\hat{\psi}_{\mathrm{m}\nu}$ can be expressed as a function of the three orthogonal invariants of $\boldsymbol{C}_{\mathrm{e}} = \boldsymbol{F}_{\mathrm{e}}^{\mathrm{T}}.\boldsymbol{F}_{\mathrm{e}}$, defined by (in the following expressions, $\boldsymbol{\eta}$ is the metric tensor associated with the natural state of the material)

$$I_{1\mathrm{e}}(\boldsymbol{C}_{\mathrm{e}}) = \mathrm{tr}(\boldsymbol{\eta}^{-1}\boldsymbol{C}_{\mathrm{e}}), \tag{A.4a}$$

$$I_{2\mathrm{e}}(\boldsymbol{C}_{\mathrm{e}}) = \tfrac{1}{2}\{I_{1\mathrm{e}}(\boldsymbol{C}_{\mathrm{e}}) - \mathrm{tr}[(\boldsymbol{\eta}^{-1}\boldsymbol{C}_{\mathrm{e}})^2]\}, \tag{A.4b}$$

$$I_{3\mathrm{e}}(\boldsymbol{C}_{\mathrm{e}}) = \det \boldsymbol{C}_{\mathrm{e}}. \tag{A.4c}$$

In this work, we adopt the Holmes&Mow model of strain energy density function [56], thereby leading to the following constitutive law for $\hat{\psi}_{\mathrm{m}\nu}$

$$\hat{\psi}_{\mathrm{m}\nu}(\boldsymbol{C}_{\mathrm{e}}) = \alpha_0\Big\{\frac{\exp(\alpha_1[I_{1\mathrm{e}}(\boldsymbol{C}_{\mathrm{e}}) - 3] + \alpha_2[I_{2\mathrm{e}}(\boldsymbol{C}_{\mathrm{e}}) - 3])}{[I_{3\mathrm{e}}(\boldsymbol{C}_{\mathrm{e}})]^{\alpha_3}} - 1\Big\}. \tag{A.5}$$

with $\alpha_0, \alpha_1, \alpha_2, \alpha_3$ being material parameters. For what concerns the fibers, the energetic term $\psi_{\mathrm{f}\nu}$ accounts for two contributions

$$\hat{\psi}_{\mathrm{f}\nu}(\boldsymbol{C}_{\mathrm{e}}) = \hat{\psi}^{(\mathrm{iso})}_{\mathrm{f}\nu}(\boldsymbol{C}_{\mathrm{e}}) + \hat{\psi}^{(\mathrm{ens})}_{\mathrm{f}\nu}(\boldsymbol{C}_{\mathrm{e}}),$$

where the term $\psi^{(\mathrm{iso})}_{\mathrm{f}\nu}$ pertains to the hyperelastic response of the fibers, supposed to be isotropic, and its constitutive expression is the same as the one reported in Equation (A.5), while the term $\psi^{(\mathrm{ens})}_{\mathrm{f}\nu}$ refers to the distribution of the fibers within the medium and to their orientation. In particular, we provide [19, 29, 33, 87]

$$\hat{\psi}^{(\mathrm{ens})}_{\mathrm{f}\nu}(\boldsymbol{C}_{\mathrm{e}}) = \int_{\mathbb{S}^2\mathscr{B}} \tfrac{1}{2} c\, \mathcal{H}(I_{4\mathrm{e}}(\boldsymbol{C}_{\mathrm{e}}, \mathfrak{m}) - 1)[I_{4\mathrm{e}}(\boldsymbol{C}_{\mathrm{e}}, \mathfrak{m}) - 1]^2 \mathcal{F}(\mathfrak{m}),$$

with c being an elastic parameter, $I_{4\mathrm{e}}(\boldsymbol{C}_{\mathrm{e}}, \mathfrak{m}) = \boldsymbol{C}_{\mathrm{e}} : \mathfrak{m} \otimes \mathfrak{m}$ being the fourth invariant of $\boldsymbol{C}_{\mathrm{e}}$, $\mathcal{H}$ being the Heaviside function defined by $\mathcal{H}(s) = 0$, for all $s \leqslant 0$ and $\mathcal{H}(s) = 1$, for all $s > 0$ and $\mathcal{F}$ being the von Mises distribution function, defined by [11, 29]

$$\mathcal{F}(\mathfrak{m}) = \breve{\mathcal{F}}(\theta; \xi) = \frac{2}{\pi} \sqrt{\frac{b(\xi)}{2\pi}} \frac{\exp(b(\xi)[\cos(2\theta) + 1])}{\operatorname{erfi}\left(\sqrt{2b(\xi)}\right)}. \tag{A.6}$$

Analogously, we write $\hat{f}(\theta, \phi) = f(\mathfrak{m})$ for any physical quantity depending on the angles θ and ϕ through $\mathfrak{m}$. In our specific case, this means that

$$f(\mathfrak{m}) = \tfrac{1}{2} c\, \mathcal{H}(I_{4\mathrm{e}}(\boldsymbol{C}_{\mathrm{e}}, \mathfrak{m}) - 1)[I_{4\mathrm{e}}(\boldsymbol{C}_{\mathrm{e}}, \mathfrak{m}) - 1]^2.$$

In Equation (A.6), the parameter b depends on material points through the normalised axial length $\xi = X^3/L$, with L corresponding to a reference dimension of the reference configuration, such that $b(\xi) = -16\xi + 8$ [87] and the function erfi denotes the Gaussian error distribution. The latter, in particular, is related to the imaginary Gaussian error distribution erfi through $\operatorname{erfi}(s) = -i\operatorname{erf}(is)$, for any real number $s \in \mathbb{R}$.

We introduce the strain energy density per unit volume of the reference configuration, $\psi_{\mathrm{R}} = J_{\mathrm{p}} \psi_\nu$, with $J_{\mathrm{p}} = 1$, and we rephrase the orthogonal invariants of $\boldsymbol{C}_{\mathrm{e}}$ in Equations (A.4) in terms of $\boldsymbol{C}$ and $\boldsymbol{B}_{\mathrm{p}} := \boldsymbol{K}.\boldsymbol{K}^{\mathrm{T}}$ i.e.,

$$I_1(\boldsymbol{C}, \boldsymbol{B}_{\mathrm{p}}) = \operatorname{tr}(\boldsymbol{B}_{\mathrm{p}} \boldsymbol{C}), \tag{A.7a}$$

$$I_2(\boldsymbol{C}, \boldsymbol{B}_{\mathrm{p}}) = \tfrac{1}{2}\{I_1(\boldsymbol{C}, \boldsymbol{B}_{\mathrm{p}}) - \operatorname{tr}[(\boldsymbol{B}_{\mathrm{p}} \boldsymbol{C})^2]\}, \tag{A.7b}$$

$$I_3(\boldsymbol{C}, \boldsymbol{B}_{\mathrm{p}}) = \det \boldsymbol{C} \det \boldsymbol{B}_{\mathrm{p}} = \det \boldsymbol{C}, \tag{A.7c}$$

so that we can write

$$\hat{\psi}_{\mathrm{mR}}(\boldsymbol{C}, \boldsymbol{B}_{\mathrm{p}}) = \alpha_0 \Big\{ \frac{\exp(\alpha_1[I_1(\boldsymbol{C}, \boldsymbol{B}_{\mathrm{p}}) - 3] + \alpha_2[I_2(\boldsymbol{C}, \boldsymbol{B}_{\mathrm{p}}) - 3])}{[I_3(\boldsymbol{C}, \boldsymbol{B}_{\mathrm{p}})]^{\alpha_3}} - 1 \Big\}, \tag{A.8a}$$

$$\hat{\psi}^{(\mathrm{ens})}_{\mathrm{fR}}(\boldsymbol{C}, \boldsymbol{K}) = \int_{\mathbb{S}^2\mathscr{B}} \tfrac{1}{2} c\, \mathcal{H}(I_4(\boldsymbol{C}, \boldsymbol{K}, \mathfrak{m}) - 1)[I_4(\boldsymbol{C}, \boldsymbol{K}, \mathfrak{m}) - 1]^2 \mathcal{F}(\mathfrak{m}), \tag{A.8b}$$

with

$$I_4(\boldsymbol{C}, \boldsymbol{K}, \mathfrak{m}) = \boldsymbol{C} : \boldsymbol{K}\mathfrak{m} \otimes \boldsymbol{K}\mathfrak{m}. \tag{A.9}$$

TABLE 2. List of the main symbols employed in the work.

Symbol	Variable	Expression
$\boldsymbol{u}$	total deformation	$\chi(X,t)-\chi(X,0)$
$\boldsymbol{F}$	deformation gradient tensor	$F^a{}_A=(D\chi)^a{}_A=\partial_A\chi^a$
$\boldsymbol{F}_\mathrm{e}$	accomodating tensor	$\boldsymbol{F}=\boldsymbol{F}_\mathrm{e}\boldsymbol{F}_\mathrm{p}$
$\boldsymbol{F}_\mathrm{p}$	remodeling tensor	$\boldsymbol{F}=\boldsymbol{F}_\mathrm{e}\boldsymbol{F}_\mathrm{p}$
$\boldsymbol{K}$	implant tensor	$\boldsymbol{K}=\boldsymbol{F}_\mathrm{p}^{-1}$
$\boldsymbol{\Lambda}$	tensor of rate of remodeling	$\dot{\boldsymbol{K}}\,\boldsymbol{K}^{-1}$
J	deformation Jacobian	$J=\det\boldsymbol{F}$
J_e	elastic Jacobian	$J=\det\boldsymbol{F}_\mathrm{e}$
J_p	remodeling Jacobian	$J=\det\boldsymbol{F}_\mathrm{p}$
$J_{\boldsymbol{K}}$	implant tensor Jacobian	$J_{\boldsymbol{K}}=\det\boldsymbol{K}$
$\boldsymbol{C}$	right Cauchy-Green tensor	$\boldsymbol{C}=\boldsymbol{F}^\mathrm{T}.\boldsymbol{F}$
$\boldsymbol{C}_\mathrm{e}$	elastic Cauchy-Green tensor	$\boldsymbol{C}_\mathrm{e}=\boldsymbol{F}_\mathrm{e}^\mathrm{T}.\boldsymbol{F}_\mathrm{e}$
ψ_R	strain energy density	Equations (A.8)
$\boldsymbol{P}$	first Piola–Kirchhoff stress tensor	$\boldsymbol{P}=\partial\psi_\mathrm{R}/\partial\boldsymbol{F}$
$\boldsymbol{S}$	second Piola–Kirchhoff stress tensor	$\boldsymbol{P}=\boldsymbol{F}\boldsymbol{S}$ (A.10)
$\boldsymbol{\Sigma}$	Mandel stress tensor	$\boldsymbol{\Sigma}=\boldsymbol{C}\boldsymbol{S}$
$\boldsymbol{\sigma}$	Cauchy stress tensor	$\boldsymbol{\sigma}=J^{-1}\boldsymbol{P}\boldsymbol{F}^\mathrm{T}$
$\mathfrak{m}$	unit vector	Equation (A.2)
$\mathfrak{a}, \boldsymbol{A}$	structural tensors	Equation (A.3)
I_1, I_2, I_3	orthogonal invariants	Equations (A.7)
I_4	fourth invariant	Equation (A.9)
ζ	flow condition	Equation (2.4)
$\mathfrak{G}$	flow rule	Equation (2.8)

We can compute the second Piola–Kirchhoff stress tensor by deriving the strain energy density with respect to $\boldsymbol{C}$, and multiplying the result by 2, thereby obtaining

$$\boldsymbol{S}=\frac{2}{J_{\boldsymbol{K}}}\varphi_{\mathrm{m}\nu}[(\beta_1+\beta_2 I_1)\boldsymbol{B}_\mathrm{p}-\beta_2\boldsymbol{B}_\mathrm{p}\boldsymbol{C}\boldsymbol{B}_\mathrm{p}+\beta_3 I_3\boldsymbol{C}^{-1}] + \frac{2}{J_{\boldsymbol{K}}}\varphi_{\mathrm{f}\nu}\int_{\mathbb{S}^2\mathscr{B}} c\,\mathcal{H}(I_4(\boldsymbol{C},\boldsymbol{K},\mathfrak{m})-1)[I_4(\boldsymbol{C},\boldsymbol{K},\mathfrak{m})-1](\boldsymbol{K}\mathfrak{a}\boldsymbol{K}^\mathrm{T})\mathcal{F}(\mathfrak{m}), \tag{A.10}$$

where β_1, β_2 and β_3 are obtained by deriving the strain energy function in Equation (A.5) with respect to I_1, I_2 and I_3, respectively. Note that, with an abuse of notation, the identiy $\boldsymbol{P}=\partial\hat{\psi}_\mathrm{R}/\partial\boldsymbol{F}=\boldsymbol{F}[2(\partial\hat{\psi}_\mathrm{R}/\partial\boldsymbol{C})]$ is understood. For explicit calculations and all the model parameters not explicitly reported in this work, the reader is referred to [19].

Acknowledgments. We thank Gabriel Wittum, KAUST, for very stimulating discussions on the subject, and Dmitry Logashenko, KAUST, for very helpful hints in the course of the debugging of the code. A. Grillo was partially funded by the *'Dipartimento di Eccellenza'*, Politecnico di Torino (Italy), Project

No. E11G18000350001. S. Di Stefano acknowledges *Regione Puglia* in the context of the REFIN research project *"Riciclo di materiali e sostenibilità: modelli di delaminazione per dispositivi laminati"* and INdAM (National Institute of High Mathematics) in the context of *"Progetto Giovani GNFM 2020-2022"*. This work is partially supported by MIUR (Italian Ministry of Education, Universities and Research) through the PRIN project n. 2017KL4EF3 entitled *"Mathematics of active materials: From mechanobiology to smart devices"* and the PRIN project n. 2020F3NCPX entitled *"Mathematics for industry 4.0 (Math4I4)."* M. M. Knodel was partially supported by the German Ministry of Economics and Technology (BMWi) trough the project HYMNE (02E11809B). M. M. Knodel, S. Di Stefano and A. Grillo also acknowledge *Fondazione Cassa di Risparmio di Torino* in the context of the funding campaign "La Ricerca dei Talenti". The authors acknowledge the HLRS Stuttgart for the supplied computing time on the HLRS Apollo Hawk supercomputer.

References

1. J. C. Simo, *Numerical analysis and simulation of plasticity*, in: P. G. Ciarlet, J. L. Lions (eds.), *Handb. Numer. Anal.* **6** (1998), 179–181, Elsevier Science, Amsterdam.
2. J. Alberty, C. Carstensen, D. Zarrabi, *Adaptive numerical analysis in primal elastoplasticity with hardening.*, Comput. Methods Appl. Mech. Eng. **171** (1999), 175–204.
3. D. Ambrosi, M. Ben Amar, C. J. Cyron, A. De Simone, A. Goriely, J. D. Humphrey, E. Kuhl, *Growth and remodelling of living tissues: perspectives, challenges and opportunities*, Journal of The Royal Society Interface **16**(157) (2019), 20190233.
4. D. Ambrosi, G. A. Ateshian, E. M. Arruda, and et al., *Perspectives on biological growth and remodeling*, J. Mech. Phys. Solids **59**(4) (2011), 863–883.
5. D. Ambrosi, F. Guana, *Stress-modulated growth*, Math. Mech. Solids **12** (2007), 319–342.
6. D. Ambrosi, A. Guillou, and E. S. Di Martino, *Stress-modulated remodelling of a non-homogeneous body*, **1**, 63–76.
7. D. Ambrosi, L. Preziosi, *On the closure of mass balance models for tumor growth*, Mathematical Models and Methods in Applied Sciences **12**(05) (2002), 737–754.
8. L Amir, M Kern, *A global method for coupling transport with chemistry in heterogeneous porous media.*, Comput. Geosci. **14**(3) (2010), 465–481.
9. F. Armero, *Formulation and finite element implementation of a multiplicative model of coupled poro-plasticity at finite strains under fully saturated conditions*, Comput. Methods Appl. Mech. Eng. **171**(3–4) (1999), 205–241.
10. H. Brezis, *Functional analysis, sobolev spaces and partial differential equations*, Springer, New York, 2011.
11. M. Carfagna, A. Grillo, *The spherical design algorithm in the numerical simulation of biological tissues with statistical fibre-reinforcement*, Comput. Vis. Sci. **18** (2017), 1–28.
12. V. Ciancio, M. Dolfin, M. Francaviglia, S. Preston, *Uniform materials and the multiplicative decomposition of the deformation gradient in finite elasto-plasticity*, J. Non-Equilib. Thermodyn. **33(3)** (2008), 199–234.
13. S. C. Cowin, *How is a tissue built?*, Journal of Biomechanical Engineering **122** (2000), 553–569.
14. S. C. Cowin, *Tissue growth and remodeling*, Annual Review of Biomedical Engineering **6**(1) (2004), 77–107.
15. E. Crevacore, S. Di Stefano, A. Grillo, *Coupling among deformation, fluid flow, structural reorganisation and fibre reorientation in fibre-reinforced, transversely isotropic biological tissues*, Int. J. Non-Linear Mech. **111** (2019), 1–13.

16. C. de Dieuleveult, J, Erhel, *A global approach to reactive transport: application to the momas benchmark*, Comput. Geosci. **14**(3) (2010), 451–464.
17. C. de Dieuleveult, J. Erhel, M. M. Kern, *A global strategy for solving reactive transport equations*, J. Comput. Phys. **228**(17) (2009), 6395–6410.
18. S. Di Stefano, E. Benvenuti, V. Coscia, *On the role of friction and remodelling in cell-matrix interactions: A continuum mechanical model*, Int. J. Non-Linear Mech. **142** (2022), 103966.
19. S. Di Stefano, M. Carfagna, M. M. Knodel, K. Hashlamoun, S. Federico, A. Grillo, *Anelastic reorganisation of fibre-reinforced biological tissues*, Comput. Vis. Sci. **20**(3-6) (2019), 95–109.
20. S. Di Stefano, G. Florio, G. Napoli, N. M. Pugno, G. Puglisi, *On the role of elasticity in focal adhesion stability within the passive regime*, Int. J. Non-Linear Mech. **146** (2022), 104157.
21. S. Di Stefano, A. Giammarini, C. Giverso, A. Grillo, *An elasto-plastic biphasic model of the compression of multicellular aggregates: the influence of fluid on stress and deformation*, Z. Angew. Math. Phys. **73**(2) (2022), 79.
22. S. Di Stefano, A. Ramírez-Torres, R. Penta, A. Grillo, *Self-influenced growth through evolving material inhomogeneities*, Int. J. Non-Linear Mech. **106** (2018), 174–187.
23. M. Epstein, *Mathematical characterization and identification of remodeling, growth, aging and morphogenesis*, J. Mech. Phys. Solids **84** (2015), 72–84.
24. M. Epstein, *The split between remodelling and aging*, Int. J. Non-Linear Mech. **44**(6) (2009), 604–609.
25. M. Epstein, G. A. Maugin, *On the geometrical material structure of anelasticity*, Acta Mech. **115**(1–4) (1996), 119–131.
26. M. Epstein, G. A. Maugin, *Thermomechanics of volumetric growth in uniform bodies*, Int. J. Plast. **16**(7–8) (2000), 951–978.
27. R. A. Eve, B. D. Reddy, *The variational formulation and solution of problems of finite-strain elastoplasticity based on the use of a dissipation function*, Int. J. Numer. Methods Eng. **37**(10) (1994), 1673–1695.
28. S. Federico, *Porous materials with statistically oriented reinforcing fibres*, in: L. Dorfmann, R. W. Ogden, (eds.), *Nonlinear Mechanics of Soft Fibrous Materials*, Springer, CISM Courses Lect. **559** (2015), 49–120.
29. S. Federico, T. C. Gasser, *Non-linear elasticity of biological tissues with statistical fibre orientation*, Journal of the Royal Society Interface **7** (2010), 955–966.
30. S. Federico, A. Grillo, *Elasticity and permeability of porous fibre-reinforced materials under large deformations*, Mechanics of Materials **44** (2012), 58–71.
31. S. Federico, A. Grillo, *Linear elastic composites with statistically oriented spheroidal inclusions*, in: S. A. Meguid, G. J. Weng (eds.), *Micromechanics and Nanomechanics of Composite Solids*, Springer International Publishing, 2017, 307–346.
32. S. Federico, A. Grillo, G. La Rosa, G. Giaquinta, W. Herzog, *A transversely isotropic, transversely homogeneous micro-structural-statistical model of articular cartilage*, Journal of Biomechanics **38** (2005), 2008–2018.
33. S. Federico, W. Herzog, *On the anisotropy and inhomogeneity of permeability in articular cartilage*, Biomechanics and Modeling in Mechanobiology **7** (2008), 367–378.
34. S. Federico, W. Herzog, *On the permeability of fibre-reinforced porous materials*, Int. J. Solids Struct. **45** (2008), 2160–2172.
35. N. I. Fischer, T. Lewis, B. J. J. Embleton, *Statistical Analysis of Spherical Data*, Cambridge University Press, Cambridge, UK, 1987.
36. Y. C. Fung, *Biomechanics. Motion, Flow, Stress, and Growth*, Springer-Verlag, New York, USA, 1990.
37. Y. C. Fung, *Stress, strain, growth, and remodeling of living organisms*, in: J. Casey, M. J. Crochet (eds.), *Theoretical, Experimental, and Numerical Contributions to the Mechanics of Fluids and Solids*, Birkhäuser, Basel, 1995, 469–482.
38. D. Garcia, P. K. Zysset, M. Charlebois, A. Curnier, *A three-dimensional elastic plastic damage constitutive law for bone tissue*, Biomech. Model. Mechanobiol. **8**(2) (2009), 149–165.

39. L. Geris, A. A. C. Reed, J. Vander Sloten, A. H. R. W. Simpson, H. Van Oosterwyck, *Occurrence and treatment of bone atrophic non-unions investigated by an integrative approach*, PLoS Comput. Biol. **6** (2010), e1000915.
40. L. Gerisa, A. Andreykiv, H. Van Oosterwyck, J. Vander Sloten, F. van Keulen, J. Duyck, I. Naert, *Numerical simulation of tissue differentiation around loaded titanium implants in a bone chamber*, Journal of Biomechanics **37** (2004), 763–769.
41. C. Giverso, S. Di Stefano, A. Grillo, L. Preziosi, *A three dimensional model of multicellular aggregate compression*, Soft Matter **15**(40) (2019), 10005–10019.
42. C. Giverso, L. Preziosi, *Modelling the compression and reorganization of cell aggregates*, Math. Med. Biol. **29**(2) (2012), 181–204.
43. C. Giverso, M. Scianna, A. Grillo, *Growing avascular tumours as elasto-plastic bodies by the theory of evolving natural configurations*, Mech. Res. Commun. **68** (2015), 31–39.
44. C. Gräser, R. Kornhuber, *Multigrid methods for obstacle problems*, J. Comput. Math. **27** (2009), 1–44.
45. C. Gräser, U. Sack, O. Sander, *Truncated nonsmooth newton multigrid methods for convex minimization problems*, in: M. Bercovier, M. J. Gander, R. Kornhuber, O. Widlund (eds.), Domain Decomposition Methods in Science and Engineering XVIII, Lect. Notes Comput. Sci. Eng. **70**, Springer, New York, 2009.
46. A. Grillo, M. Carfagna, S. Federico, *An Allen–Cahn approach to the remodelling of fibre-reinforced anisotropic materials*, J. Eng. Math. **109**(1) (2018), 139–172.
47. A. Grillo, S. Di Stefano, A. Ramírez-Torres, M. Loverre, *A study of growth and remodeling in isotropic tissues, based on the Anand-Aslan-Chester theory of strain-gradient plasticity*, GAMM-Mitt. **42**(4) (2019), e201900015.
48. A. Grillo, S. Federico, G. Wittum, *Growth, mass transfer, and remodeling in fiber-reinforced, multi-constituent materials*, Int. J. Non-Linear Mech. **47** (2012), 388–401.
49. A. Grillo, R. Prohl, G. Wittum, *A poroplastic model of structural reorganisation in porous media of biomechanical interest*, Contin. Mech. Thermodyn. **28** (2016), 579–601.
50. A. Grillo, G. Wittum, A. Tomic, S. Federico, *Remodelling in statistically oriented fibre-reinforced materials and biological tissues*, Math. Mech. Solids **20**(9) (2015), 1107–1129.
51. A. Grillo, R. Prohl, G. Wittum, *A generalised algorithm for anelastic processes in elastoplasticity and biomechanics*, Math. Mech. Solids **22**(3) (2017), 502–527.
52. A. Guillou, R. W. Ogden, *Growth in soft biological tissue and residual stress development*, in: G. A. Holzapfel, R. W. Ogden (eds.), *Mechanics of Biological Tissue*, Springer-Verlag, 2006, 47–62.
53. W. Han, B. D. Reddy, *Plasticity – Mathematical Theory and Numerical Analysis*, Springer, New York, 1999.
54. Apollo Hawk, HLRS Stuttgart, https://www.hlrs.de/solutions/systems/hpe-apollo-hawk.
55. I. Heppner, M. Lampe, A. Nägel, S. Reiter, M. Rupp, A. Vogel, G. Wittum, *Software framework ug4: Parallel multigrid on the hermit supercomputer*, in: W. E. Nagel, D. H. Kröner, M. M. Resch (eds.), *High Performance Computing in Science and Engineering '12*, Springer, Berlin, Heidelberg, 2012.
56. M. H. Holmes, V. C. Mow, *The nonlinear characteristics of soft gels and hydrated connective tissues in ultrafiltration.*, Journal of biomechanics **23** (1990), 1145–1156.
57. S. Hüber, B. Wohlmuth, *A primal–dual active set strategy for non-linear multibody contact problems*, Comput. Methods Appl. Mech. Eng. **194** (2005), 3147–3166.
58. T. J. R. Hughes, *The Finite Element Method: Linear Static and Dynamic Finite Element Analysis*, Prentice-Hall, Inc., Englewood Cliffs, New Jersey, 1987.
59. P. Knabner, L. Angermann, *Numerical Methods for Elliptic and Parabolic Partial Differential Equations*, Springer, Cham, 2021.
60. M. M. Knodel, S. Kräutle, P. Knabner, *Global implicit solver for multiphase multicomponent flow in porous media with multiple gas components and general reactions*, Comput. Geosci. **26** (2022), 697–724.

61. M. M. Knodel, A. Nägel, S. Reiter, M. Rupp, A. Vogel, P Targett-Adams, E. Herrmann, G. Wittum, *Multigrid analysis of spatially resolved hepatitis c virus protein simulations*, Comput. Vis. Sci. **17**(5) (2015), 235–253.
62. H. Kothari, R. Krause, *A generalized multigrid method for solving contact problems in lagrange multiplier based unfitted finite element method*, Comput. Methods Appl. Mech. Eng. **392** (2022), 114630.
63. R. Krause, B. Wohlmuth, *Monotone methods on nonmatching grids for nonlinear contact problems*, SIAM J. Sci. Comput. **25** (2003), 324–347.
64. E. Kröner, *Allgemeine Kontinuumstheorie der Versetzungen und Eigenspannungen*, Arch. Ration. Mech. Anal. **4**(1) (1959), 273–334.
65. Y. Lanir, *Constitutive equations for fibrous connective tissues*, Journal of Biomechanics **16** (1983), 1–12.
66. T. Laursen, *Computational Contact and Impact Mechanics*, Springer, New York, 2003.
67. T. Laursen, J. Simo, *A continuum-based finite element formulation for the implicit solution of multibody, large deformation frictional contact problems*, Int. J. Numer. Meth. Engrg. **36** (1993), 3451–3485.
68. V. A. Lubarda, A. Hoger, *On the mechanics of solids with a growing mass*, International Journal of the Mechanics and Physics of Solids **39** (2002), 4627–4664.
69. J. Lubliner, *Plasticity Theory*, Dover Publications, Inc., Mineola, New York, 2008.
70. J. E. Marsden, T. J. R. Hughes, *Mathematical Foundations of Elasticity*, Dover Publications Inc., Mineola, New York, 1983.
71. G. A. Maugin, M. Epstein, *Geometrical material structure of elastoplasticity*, Int. J. Plasticity **14**(1–3) (1998), 109–115.
72. M. Mićunović, *Thermomechanics of Viscoplasticity: Fundamentals and Applications*, Springer, New York, 2009.
73. T. Olsson, A. Klarbring, *Residual stresses in soft tissue as a consequence of growth and remodeling: application to an arterial geometry*, Eur. J. Mech., A, Solids **27**(6) (2008), 959–974.
74. V. Peiffer, A. Gerisch, D. Vandepitte, H. Oosterwyck, L. Geris, *A hybrid bioregulatory model of angiogenesis during bone fracture healing*, Biomech. Model. Mechanobiol. **10** (2011), 383–395.
75. A. Popp, M. Gee, W. Wall, *Finite deformation contact based on 3d dual mortar and semi–smooth newton approach*, in: G. Zavarise, P. Wriggers (eds.), *Trends in Computational Contact Mechanics*, Springer, New York, 2010, 57–77.
76. P Prendergast, P. E. Galibarov, C. Lowery, A. B. Lennon, *Computer simulating a clinical trial of a load-bearing implant: An example of an intramedullary prosthesis*, J. Mech. Beh. Biomed. Mat. **4** (2011), 1880-1887.
77. S. Preston, M. Elżanowski, *Material uniformity and the concept of the stress space*, in: B. Albers (ed.), *Continuous Media with Microstructure*, Springer Berlin Heidelberg, 2010, 91–101.
78. L. Preziosi, D. Ambrosi, C. Verdier, *An elasto-visco-plastic model of cell aggregates*, J. Theor. Biol. **262**(1) (2010), 35–47.
79. M. Puso, T. Laursen, *A mortar segment-to-segment contact method for large deformation solid mechanics*, Comput. Methods Appl. Mech. Eng. **193** (2004), 601–629.
80. S. Reiter, D. Logashenko, A. Vogel, G Wittum, *Mesh generation for thin layered domains and its application to parallel multigrid simulation of groundwater flow.*, Comput. Visual Sci. **23** (2020), 2.
81. S. Reiter, A. Vogel, I. Heppner, M. Rupp, G. Wittum, *A massively parallel geometric multigrid solver on hierarchically distributed grids*, Comput. Visual Sci. **16** (2013), 151–164.
82. Sebastian Reiter, http://www.promesh3d.com/, 2014.
83. E. K. Rodríguez, A. Hoger, A. D. McCullogh, *Stress-dependent finite growth in soft elastic tissues*, Journal of Biomechanics **27** (1994), 455–467.
84. S. Sadik, A. Yavari, *On the origins of the idea of the multiplicative decomposition of the deformation gradient*, Math. Mech. Solids **22**(4) (2017), 771–772.
85. J. C. Simo, T. J. R. Hughes, *Computational Inelasticity*, Springer, New York, 1998.

86. L. A. Taber, *Biomechanics of growth, remodeling, and morphogenesis*, Appl. Mech. Rev. **48**(8) (1995), 487–545.
87. A. Tomic, A. Grillo, S. Federico, *Poroelastic materials reinforced by statistically oriented fibres-numerical implementation and application to articular cartilage*, IMA J. Appl. Math. **79** (2014), 1027–1059.
88. M. Tur, F. Fuenmayor, P. Wriggers, *A mortar-based frictional contact formulation for large deformations using lagrange multipliers*, Comput. Methods Appl. Mech. Eng. **198** (2009), 2860–2873.
89. C. Verdier, J. Etienne, A. Duperray, L. Preziosi, *Review: Rheological properties of biological materials*, Comptes Rendus Physique **10**(8) (2009), 790–811.
90. A. Vogel, S. Reiter, M. Rupp, A. Nägel, G. Wittum, *Ug 4: A novel flexible software system for simulating pde based models on high performance computers*, Comput. Vis. Sci. **16**(4) (2013), 165–179.
91. B. Wohlmuth, *Variationally consistent discretization schemes and numerical algorithms for contact problems*, Acta Numerica **20** (2011), 569–734.
92. J. Youett, O. Sander, R. Kornhuber, *A globally convergent filter-trust-region method for large deformation contact problems*, SIAM J. Sci. Comput. **41**(1) (2019), B114–B138.

ЕФИКАСАН АЛГОРИТАМ ЗА БИОМЕХАНИЧКЕ ПРОБЛЕМЕ ЗАСНОВАН НА ПОТПУНО ИМПЛИЦИТНОМ ЊУТНОВОМ РЕШАВАЧУ

Резиме. Нумеричке симулације динамике меких биолошких ткива су изразито нетривијалне. Ткива генерално показују сложени биолошки одговор на спољашња и унутрашња дејства, укључујући велике деформације и ремоделирање. Комбинујући предности решавача глобално имплицитног приступа (GIA) са општом примењивости полуимплицитног општег алгоритма пластичности (GPA), представљамо нови ефикасан алгоритам пластичности. Алгоритам пластичности на бази биомеханике (BMBPA) је потпуно имплицитан, заснован на угнежђеном Њутновом решавачу и природно је погодан за масовна паралелна израчунавања.

При увођењу непознатих величина модела коришћена је Билби-Кронер-Ли (BKL) мултипликативна декомпозиција тензора градијента деформације. Разликујемо глобалне и локалне непознате, придружене локалним и глобалним једначинама, које су повезане помоћу функције резолуције. BMBPA тражи врло мало услова за примену и стога се може лако користити за решавање неколико врста биолошких и биомеханичких проблема. Показали смо ефикасност BMBPA извођењем два нумеричка експеримента монофазног модела ткива ојачаних влакнима.

У једном случају разматрамо тест смицања-компресије кубичног узорка ткива, док се у другом случају фокусирамо на тест неограничене компресије цилиндра. BMBPA је способан да реши деформацију и ремоделирање анизотропних биолошких ткива користећи време рачунања у сатима, док GPA, примењен на исте проблеме као и BMBPA, треба знатно дуже време. Сви прорачуни су обављени паралелно и, у оквиру свих тестова, перформансе BMBPA су биле знатно веће од перформанси GPA. Резултати симулација омогућавају проучавање укупног механичког понашања разматраног ткива и омогућавају даља истраживања у области биомеханике ткива.

Goethe Center for Scientific Computing (GCSC)
Universität Frankfurt
Frankfurt am Main
Germany
markus.knodel@gcsc.uni-frankfurt.de

(Received 15.11.2022)
(Revised 22.12.2022)
(Available online 28.12.2022)

Dipartimento di Ingegneria Civile, Ambientale, del Territorio, Edile e di Chimica
Politecnico di Bari
Bari
Italy
salvatore.distefano@poliba.it

Goethe Center for Scientific Computing (GCSC)
Universität Frankfurt
Frankfurt am Main
Germany
naegel@gcsc.uni-frankfurt.de

Dipartimento di Scienze Matematiche “G. L. Lagrange” (DISMA)
Politecnico di Torino
Torino
Italy
alfio.grillo@polito.it